NASA Technical Paper 1027

Effects of Roughness Size on the Position of Boundary-Layer Transition and on the Aerodynamic Characteristics of a 55° Swept Delta Wing at Supersonic Speeds

Robert L. Stallings, Jr., and Milton Lamb

DECEMBER 1977

NASA

NASA Technical Paper 1027

Effects of Roughness Size on the Position of Boundary-Layer Transition and on the Aerodynamic Characteristics of a 55° Swept Delta Wing at Supersonic Speeds

Robert L. Stallings, Jr., and Milton Lamb
Langley Research Center
Hampton, Virginia

National Aeronautics
and Space Administration

**Scientific and Technical
Information Office**

1977

SUMMARY

An experimental investigation has been conducted to determine the effects of roughness size on the position of boundary-layer transition and on the aerodynamic characteristics of a 55^{o} swept-delta-wing model. The tests were conducted at free-stream Mach numbers from 1.50 to 4.63, Reynolds numbers per meter from 3.3×10^{6} to 1.6×10^{7}, angles of attack from -8^{o} to 16^{o}, and roughness sizes ranging from 0.027-cm sand grit to 0.127-cm-high cylinders.

Near 0^{o} angle of attack, effective roughness Reynolds numbers for the model used in this investigation were generally less than existing flat-plate results at similar free-stream conditions. Within the frequency range of the thin-film gauge instrumentation used in the tests (≈15 kHz), roughness size had little or no effect on turbulence level at the model surface once fully turbulent flow was established.

Increasing the angle of attack caused the transition to move downstream on the model leeward surface and upstream on the windward surface. At a Mach number of 4.63 and a 16^{o} angle of attack, large regions of laminar flow occurred on the model leeward surface for all roughness sizes tested.

An empirical method was derived for predicting the drag of roughness elements used in boundary-layer trips and results from the method are in good agreement with measured values near zero lift. Experimental results from the tests performed in this investigation indicate drag increment due to roughness remains approximately constant with changes in angle of attack up to the maximum angles tested.

For the full range of test variables, grit size had little or no effect on lift coefficient and pitching moment. Significant effects of grit size were observed on drag coefficient and lift-drag ratio.

INTRODUCTION

Limitations in size and unit Reynolds number capability of most continuous-flow, supersonic wind tunnels generally require the use of artificial roughness, commonly referred to as boundary-layer trips, to promote fully turbulent boundary-layer conditions over surfaces of models. The experimental aerodynamicist is frequently confronted with the problem of selecting a boundary-layer trip that is sufficiently large to insure that the boundary layer is effectively tripped but not so large that the boundary-layer and local

flow conditions will be distorted. Selection of grit size is further complicated by the current policy of operating wind tunnels at reduced unit Reynolds numbers to meet the national goals of reduced energy consumption.

Numerous investigations have been conducted, with results available in the literature, to serve as guides for selecting the correct boundary-layer trip for given test conditions. For example, references 1, 2, and 3 summarize techniques for selecting trip sizes for subsonic, supersonic, and hypersonic speed ranges, respectively. Data presented in these references as well as most other data in the literature are generally limited to zero-pressure-gradient bodies such as cones and flat plates. Very few data are available to indicate the effects of pressure gradient, angle of attack, wing sweep, etc., on roughness required to fix transition. Since most practical wind-tunnel models incorporate all these variables, the magnitude of their effects must be determined before the zero-pressure-gradient results can be confidently applied. This investigation was initiated to provide a data base for some of these effects. An additional objective of the investigation was to evaluate the technique of predicting drag of the boundary-layer trips described in references 4 and 5 when applied to a three-dimensional body.

An existing 55° swept-delta-wing model with a 4-percent-thick circular-arc airfoil was used in the investigation. This model was one of a family of models previously tested in the Langley Unitary Plan wind tunnel (ref. 6). For the present tests which were conducted in the same facility, boundary-layer transition location and force and moment data were obtained for roughness sizes ranging from 0.027-cm sand grit to 0.127-cm-high cylinders at Mach numbers from 1.50 to 4.63, Reynolds numbers per meter from 3.3×10^6 to 1.6×10^7, and angles of attack from approximately -8° to 16°. Both surface thin-film gauges (ref. 7) and the sublimation technique (ref. 8) were used to define the location of transition. The force and moment data were obtained by using a standard six-component strain-gauge balance.

SYMBOLS

A_c projected frontal area of individual roughness element, m^2

C_A model axial-force coefficient, $\frac{\text{Axial force}}{q_\infty S}$

C_D model drag-force coefficient, $\frac{\text{Drag force}}{q_\infty S}$

$C_{D,C}$ drag coefficient of element used in transition strip, $\frac{\text{Drag force}}{q_\infty A_c}$

$C_{D,IC}$ drag coefficient of isolated cylinder or isolated roughness element, $\frac{\text{Drag force}}{q_\infty A_c}$

$C_{D,o}$ model drag coefficient at zero lift, $\frac{\text{Drag force}}{q_\infty S}$

C_L model lift coefficient, $\frac{\text{Lift}}{q_\infty S}$

C_m pitching-moment coefficient, $\frac{\text{Pitching moment}}{q_\infty S\bar{c}}$

$\bar{c}$ mean aerodynamic chord, 36.35 cm

E_{rms} root mean square of voltage fluctuation, mV

$g(\Lambda,M_\infty)$ term in equations (4) and (5) to account for sweep angle and Mach number effects

k roughness height, cm

L/D lift-drag ratio

l length of transition strip, cm

M_∞ free-stream Mach number

N number of roughness elements

q_∞ free-stream dynamic pressure, N/m^2

R free-stream Reynolds number per meter, U/ν, m^{-1}

R_k roughness Reynolds number, $0.01\frac{Uk}{\nu}$

R'_k roughness parameter, equation (1)

$R_{k,eff}$ roughness Reynolds number required to move transition near vicinity of boundary-layer trip, $0.01\frac{Uk}{\nu}$

$R_{x,k}$ Reynolds number based on chordwise distance from leading edge to location of boundary-layer trip, $0.01 \frac{Ux_k}{\nu}$

$R_{x,t}$ Reynolds number based on chordwise distance from leading edge to location of transition, $0.01 \frac{Ux_t}{\nu}$, $0.01 \frac{Ux_{t,0}}{\nu}$

S model planform area, 0.2045 m^2

s roughness spacing measured from center to center of elements, cm

T_{aw} adiabatic wall temperature, K

T_k temperature at roughness height, K

T_w wall temperature, K

U free-stream velocity, m/sec

w width or diameter of roughness elements, cm

x chordwise distance from leading edge, cm

x_k location of transition strip, cm

x_t location of roughness induced transition (peak root-mean-square voltage from thin-film gauge), cm

$x_{t,0}$ location of natural transition (peak root-mean-square voltage from thin-film gauge), cm

α angle of attack, deg

δ_k boundary-layer thickness at $x = x_k$, cm

δ^*_k boundary-layer displacement thickness at $x = x_k$, cm

ϵ value of R'_k where $x_t = x_k$

Λ leading-edge sweep angle, deg

ν free-stream kinematic viscosity, m^2/sec

ω exponent in viscosity-temperature relation, equation (1)

APPARATUS AND METHODS

Tunnel

The tests were conducted in both the low and high Mach number test sections of the Langley Unitary Plan wind tunnel which is a variable pressure continuous flow facility (ref. 9). The asymmetric sliding-block nozzles lead to the test sections and permit a continuous variation in Mach number from about 1.5 to 2.9 in the low Mach number test section and from about 2.3 to 4.7 in the high Mach number test section.

Model

Details of the model used in the investigation are shown in figure 1. The model consists of a clipped 55° swept delta wing with a 4-percent-thick circular-arc airfoil. A body of revolution was added symmetrically about the wing center line to provide a housing for the strain-gauge balance. The base diameter was 5.08 cm and was the minimum diameter required to house the balance.

TEST CONDITIONS

Tests were conducted at the following test conditions:

Mach number	Stagnation temperature, K	Stagnation pressure range, kN/m^2	Reynolds number range, m^{-1}
1.50	339	27 to 133	3.3×10^6 to 1.6×10^7
2.36	339	38 to 189	
2.86	339	49 to 246	
3.95	352	92 to 460	
4.63	352	126 to 631	

The dewpoint temperature at stagnation conditions was maintained below 239 K to insure negligible condensation effects.

The effectiveness of transition strips containing roughness sizes ranging from 0.027-cm sand grit elements to 0.127-cm high cylinder was investigated. The size of the sand elements was determined by sifting sand elements of various sizes through a stack of U.S. Standard sieves. The sieves were arranged according to size, with the largest-mesh sieve at the top of the stack and the sieves with progressively smaller mesh toward the bottom. The size of the sand elements resting on a collecting sieve was determined by averaging the size of the mesh openings of that collecting sieve and the size of the mesh openings of the preceding sieve through which the elements had passed. The sieve number, mesh openings, and nominal particle sizes are given in the following table:

Sieve number	Mesh opening, cm	Nominal particle size collected, k, cm
20	0.0841	
25	.0711	0.0776 ± 0.0065
30	.0589	.0650 ± .0061
35	.0500	.0545 ± .0045
40	.0419	.0460 ± .0041
45	.0351	.0385 ± .0034
50	.0297	.0324 ± .0027
60	.0249	.0273 ± .0024

The cylindrical elements were machined from small copper rods and were 0.127 cm in diameter and 0.127 cm in length. All transition strips were located 1.02 cm aft of the leading edge measured in a streamwise direction. For the transition strips containing the smaller roughness elements (k = 0.027, 0.032 cm), the elements were randomly spaced in a band (approximately 0.159 cm wide) parallel to the leading edge. All other transition strips contained single spaced elements that were arranged in a line parallel to the leading edge and located at intervals determined from the equation

$$s = \frac{4k}{\cos \Lambda}$$

MEASUREMENTS AND INSTRUMENTATION

Strain-Gauge Balance

Aerodynamic forces and moments were measured by means of a six-component electrical strain-gauge balance housed within the model. The balance was rigidly fastened to a sting support system. Balance-chamber pressure was determined by averaging measurements from two static pressure orifices located in the vicinity of the balance.

Thin-Film Gauges

After completion of the force and moment tests, the model was instrumented with surface thin-film gauges. Each gauge consisted of a thin platinum coating on the end of a quartz rod. At 273 K the resistance of the gauges was approximately 5.5 ohms. Gauges were mounted at 10 locations on the model by cementing the quartz rods in 0.153-cm-diameter holes that were drilled perpendicular to the model surface (fig. 1). That end of the quartz rod with the platinum film was located flush with the model upper surface.

The gauges were operated in a constant temperature mode at an overheat ratio of approximately 1.5. A switch assembly was used to connect each gauge into a single-channel anemometer system, and the bridge voltage output fluctuation of the system was measured by using a true root-mean-square (rms) meter.

Typical rms bridge voltages from the present tests for the thin-film gauges are shown in figure 2 for both natural boundary-layer transition and roughness induced transition. Oscilloscope traces of the bridge voltage fluctuations are also shown for comparison with the measured rms voltages at selected Reynolds numbers. The variation in rms voltages shows an increase in fluctuation level with increasing Reynolds number from a level corresponding to laminar flow at the lower Reynolds numbers to a level corresponding to turbulent flow at the higher Reynolds numbers and a peak value corresponding to transitional flow at the intermediate Reynolds numbers. For the present tests, transition Reynolds numbers are based on the unit Reynolds numbers corresponding to the peak fluctuation level, which as discussed in reference 7, should give results consistent with values based on peak surface pitot pressure or peak surface temperatures.

For the case of natural transition, figure 2(a) shows large positive voltage pulses on the oscillograph trace at Reynolds numbers slightly less than the peak voltage

Reynolds number; large negative pulses are shown on the trace at Reynolds numbers slightly greater than the peak voltage Reynolds number. The positive pulses are believed to result from turbulent bursts intermittently increasing the heat transfer rate from the gauge. These bursts require an increase in bridge voltage to maintain the constant temperature condition. Conversely, the negative pulses are believed to result from intermittent laminar flow occurring at the gauge in an otherwise predominantly turbulent boundary layer. With further increases in Reynolds number, the location of transition moves upstream of the gauge. Random positive and negative fluctuations representative of turbulent flow then result.

For the case of forced (roughness-induced) transition, the peak in rms voltage indicative of transition was much lower than the peak for natural transition (fig. 2(b)). In some cases no peak at all was observed; however, a definite change in rms voltage level indicative of the change from laminar to turbulent flow always occurred when transition moved upstream of the gauge. For these cases, the Reynolds number corresponding to the initial onset of the increased voltage level was defined as the transition Reynolds number. Although the measurements of reference 7 always indicated a distinctive peak for forced transition, the peak occurred just ahead of the initial onset of the increased fluctuation associated with fully turbulent flow over a very narrow band of Reynolds numbers. Therefore, the definition of transition Reynolds number for the present data where no peak was observed is not believed to be significantly inconsistent with the technique developed in reference 7.

Sublimation

Limited tests were also conducted using the sublimation technique for detecting the location of boundary-layer transition. This technique is described in detail in reference 8.

CORRECTIONS

For the force and moment tests, angles of attack have been corrected for tunnel-flow misalignment and for deflection of the sting and balance caused by aerodynamic loads. Drag coefficients were adjusted to correspond to free-stream static pressure conditions at the base of the model.

During the thin-film tests, the model was placed at the same location in the test sections as it was for the force balance tests. Therefore, the tunnel-flow misalignment determined from the force balance tests was used to correct angle of attack for the thin-film tests. No corrections were made to angle of attack for aerodynamic loads during

the thin-film tests; however, this effect was minimized by the use of a sting that was shorter and larger in diameter than the sting used for the force tests. This sting was rigidly attached to the model.

RESULTS AND DISCUSSION

Thin-Film Data

As shown in figure 1, the model was instrumented with thin-film gauges at two spanwise stations; however, for the sake of clarity and consistency, results are presented only for the more extensively instrumented inboard station. When transition was located within the instrumentation regions of the outboard station, these results generally agreed well with measurements obtained at the inboard station. This agreement indicates that the transition front paralleled the wing leading edge. This parallelism was, in fact, substantiated by the sublimation data.

Thin-film data are not presented for Mach 1.5. During the initial thin-film runs at this Mach number, it became apparent that the subsonic leading edge permitted disturbances created by the forward gauges protruding through the lower surface to contaminate the flow over the upper surface. Therefore, further testing of the thin-film gauges at this Mach number was discontinued. At the higher test Mach numbers, the leading edge was supersonic, and no indication of contaminated flow over the upper surface was observed.

Shown in figure 3 are natural transition results for the range of unit Reynolds number and Mach numbers from 2.36 to 4.63. Limited sublimation data that were obtained are shown as the primed symbols and generally agree well with the thin-film data. The variation of $x_{t,0}$ with unit Reynolds number and Mach number is somewhat similar to trends reported in the literature for flat plates and cones. The variation of $R_{x,t}$ with unit Reynolds number at the higher Mach numbers, however, is not consistent with existing flat-plate and cone data. Extensive wind-tunnel testing of these zero pressure gradient bodies has shown that $R_{x,t}$ increases with increasing unit Reynolds number contrary to the results shown in figure 3. This unit Reynolds number effect is generally attributed to wind-tunnel noise radiated from the nozzle sidewall boundary layer. Several investigators (see, for example, ref. 10) have derived empirical equations that correlate transition data from various wind tunnels that collectively have a wide range of radiated noise levels. Unpublished transition data from a hollow cylinder model and a 10° cone model tested in the Langley Unitary Plan wind tunnel when expressed in terms of the correlation parameters in reference 10 are in good agreement with data from other facilities. Therefore, the trends shown in figure 3 probably

do not result from tunnel effects but from three-dimensional effects created either by the delta wing itself or by an interaction between the flow field over the delta wing and the body section that houses the balance and sting.

Shown in figure 4 is the effect of angle of attack on the location of natural transition for Mach numbers from 2.36 to 4.63. The ordinate parameter is the distance to transition at angle of attack nondimensionalized by the distance to transition at 0^{o} angle of attack. The results show that on the windward side of the model, transition moves upstream toward the wing leading edge with increasing angle of attack; whereas on the leeward side, transition moves downstream with increasing angle of attack. The results also indicate that the nondimensional transition location parameter becomes less sensitive to angle of attack with increasing Mach number.

Presented in figure 5 is the effect of grit size on the location of boundary-layer transition. As expected, the effectiveness of a given grit size for inducing transitional flow decreases with increasing Mach number. At Mach numbers 2.36 and 2.86, data were obtained for k ranging from 0.027 cm to 0.055 cm; at Mach numbers 3.95 and 4.63, results were obtained for k ranging from 0.055 cm to 0.127 cm. At Mach number 2.36 considerable data scatter occurred and a clear trend of the variation of x_t with k was not established. At the higher test Mach numbers, the effect of k is readily apparent from the data and consists of the anticipated upstream movement of transition with increasing k. Sublimation data, shown as the primed symbols in figure 5, generally agree well with the thin-film data.

In reference 11, roughness-induced transition data for flat plates and cones are correlated by using a roughness parameter defined as

$$R'_k = R_k\left(\frac{T_k}{T_w}\right)^{0.5+\omega} \tag{1}$$

Since R'_k must be calculated at a station x_k rather than at x_t, the investigators reasoned that the effectiveness of the roughness would vary according to the distance between roughness and transition. The quantity

$$\sqrt{\frac{x_t}{x_{t,0}}} - \sqrt{\frac{x_k}{x_{t,0}}}\left(\frac{R'_k}{\epsilon}\right) \tag{2}$$

was selected to represent these relative positions for flow having zero pressure gradient. The constant ϵ represents the value of R'_k where $x_t = x_k$. In references 3 and 12, data are correlated using the parameters defined by equations (1) and (2) in the form

$$\frac{R'_k}{\epsilon} = f\left[\sqrt{\frac{x_t}{x_{t,0}}} - \sqrt{\frac{x_k}{x_{t,0}}}\left(\frac{R'_k}{\epsilon}\right)\right] \tag{3}$$

where a value of ϵ was selected that best correlated the data of references 3 and 12 for a given Mach number. Data from the present tests were also correlated using the parameters from equation (3). Values of ϵ of 1500 at Mach 2.36 and 2.86 and values of ϵ of 2000 at Mach 3.95 and 4.63 seemed to give the least data scatter. These results are shown in figure 6 for the test range of Mach numbers for values of k greater than the boundary-layer thickness calculated by assuming zero pressure gradient conditions over the distance x_k. This latter restriction $(k \geq \delta_k)$ was imposed due to the sensitivity of R'_k to k for $k < \delta_k$ and the unknown error in δ_k resulting from the assumption of a zero pressure gradient. The reduced values of ϵ used in the correlation of the present data in addition to the fact that the data level falls below the flat-plate data indicate that roughness more effectively trips the boundary layer for the present configuration.

Effective roughness Reynolds numbers for the present tests are shown in figure 7 and are compared with existing flat-plate data. The effective roughness Reynolds numbers for the present tests are defined as the product of roughness height and the free-stream unit Reynolds number required to move transition to the first thin-film gauge located downstream of the transition strip. Based on the data shown in figure 5, this definition should be consistent with effective roughness Reynolds numbers determined from the "knee-of-the-curve" technique discussed in reference 3. Results from the present tests fall below both flat-plate curves shown in figure 7; however, the curves representing data of reference 3 are closer to the present data, particularly at the higher Mach numbers. The differences in the values of $R_{k,\mathrm{eff}}$ for references 3 and 12 could be due to different techniques of defining $R_{k,\mathrm{eff}}$ or possibly to an effect of $R_{x,k}$ on $R_{k,\mathrm{eff}}$ that is shown in figure 6 of reference 3, but is not apparent from the data of reference 12.

The effect of angle of attack on the location of roughness-induced transition is shown in figure 8 for Mach 2.36 to 4.63 at a constant unit Reynolds number per meter of 6.56×10^6. Results obtained on the leeward side of the model are presented in figure 8(a) for the minimum and maximum roughness size tested at this Reynolds number and at angle of attack. With increasing angle of attack, the results show a downstream movement of transition which increases with increasing Mach number and decreasing roughness size. The results show that at Mach 4.63 even the 0.127-cm-high cylinders were not sufficiently large to retain the location of transition near the vicinity of the transition strip for any significant range of angles of attack. This sensitivity of transition location with angle of attack could significantly affect the onset of boundary-layer

separation that occurs in regions of adverse pressure gradients as, for example, those created by aerodynamic control surfaces. Therefore, caution should be applied in interpreting aerodynamic data (such as control effectiveness, etc.) obtained in wind tunnels at high Mach numbers and at large angles of attack. The increase in the extent of laminar flow on the leeward surface also results in a reduction in skin-friction drag; however, as discussed subsequently, the skin-friction drag at an angle of attack is apparently dominated by the friction drag on the windward surface. The effect of increasing the angle of attack on the position of transition for the windward side of the model (fig. 8(b)) consists of a forward movement toward the transition strip. Therefore, if the boundary layer is adequately tripped near the transition strip at $\alpha = 0^{\circ}$, only small changes in the location of transition should occur on windward surfaces with increasing angle of attack.

Shown in figure 9 is the effect of k on the rms voltages at instrumentation locations ranging from the most forward gauge to the most aft gauge. No significance is placed on the magnitude of these measurements other than to indicate that once fully turbulent flow is established, roughness size has little or no effect on the turbulence intensity at the wall. This lack of sensitivity to roughness is somewhat surprising since numerous investigators (see, for example, ref. 13) have shown that large lateral shear gradients occur downstream of large roughness elements. Part of this lack of sensitivity could result from the limited frequency response of the anemometer system used for the present tests. The upper frequency limit (-3 dB) of the system as determined by the conventional square wave technique was approximately 15 kHz.

Force Balance Data

The effects of roughness on drag coefficients at zero lift are shown in figure 10 for the test range of Mach number. The shape of the $C_{D,o}$ curves are strongly influenced by the position of boundary-layer transition. For the smaller grit sizes and lower Reynolds numbers at $M_{\infty} \geq 2.36$, transition is located at some distance downstream from the trip location, and reduced values of $C_{D,o}$ are obtained. As Reynolds number is increased, transition moves upstream with turbulent flow covering a larger surface area. An increase in friction drag then results and hence an increase in $C_{D,o}$. As transition approaches the region of the trip, a peak occurs in the $C_{D,o}$ curves and further increases in Reynolds number result in a decrease in $C_{D,o}$. Increasing grit size results in a reduction in the peak $C_{D,o}$ Reynolds number and also an increase in the level of $C_{D,o}$ as a result of the grit wave drag. The minimum test Reynolds number at Mach 1.5 was not sufficiently low to define clearly a peak in the $C_{D,o}$ curves for the range of grit sizes tested.

The crosshatched band crossing the $C_{D,o}$ curves of figure 10 at $M_\infty \geqq 2.36$ represents Reynolds numbers obtained from figure 5 at which transition is located at the first thin-film gauge (x = 2.54 cm) downstream of the transition strip. At all three Mach numbers, this crosshatched band crosses the $C_{D,o}$ curves at Reynolds numbers greater than the peak $C_{D,o}$ Reynolds number. Reynolds numbers required to move transition to the second instrumentation station (x = 5.08 cm), as determined from figure 5, more closely approximate the peak $C_{D,o}$ Reynolds numbers of figure 10. These results imply that zero-lift drag measurements representative of fully turbulent flow can be obtained with transition located at some small distance downstream of the transition strip. Conversely, the results indicate that the peak $C_{D,o}$ Reynolds number is not a very good indication of when boundary-layer transition occurs at the transition strip.

It is apparent from the results shown in figures 5 and 10 that at the higher Mach numbers large roughness elements are required to induce fully turbulent flow. Under these conditions, the extraneous drag created by the elements becomes a significant part of the total model drag near zero lift. In the literature (see ref. 2, for example) several methods are described to determine the magnitude of this element drag at the low supersonic Mach numbers; however, these methods generally require additional wind-tunnel testing either through a range of Reynolds numbers or through a range of element sizes. Because of the difficulty with fixing transition at higher supersonic Mach numbers, and because of the Reynolds number limitation of most supersonic wind tunnels, the application of these methods at the higher Mach numbers could result in inaccurate results as well as an excessive amount of wind-tunnel operation.

An empirical method for predicting the drag of roughness elements used in boundary-layer trips is described in the appendix. This method is based on drag measurements of small cylinders presented in references 4 and 5; its application does not require additional wind-tunnel tests. Equations for predicting grit drag increment as derived in the appendix are

$$\Delta C_D = (5 \times 10^{-6}) \frac{l}{S} \frac{k^2}{\delta^*_k} g(\Lambda, M_\infty) \qquad \left(\frac{k}{\delta^*_k} \leqq 5\right) \tag{4}$$

and

$$\Delta C_D = (2.5 \times 10^{-5}) \frac{l}{S} k\, g(\Lambda, M_\infty) \qquad \left(\frac{k}{\delta^*_k} > 5\right) \tag{5}$$

where

$$g(\Lambda, M_\infty) = (\cos \Lambda)\left[1 - (0.0478 + 0.0430M_\infty)\cos \Lambda - (0.0341 + 0.0307M_\infty)\cos^2 \Lambda\right]$$

$$\times \left\{\cos\left[\frac{\Lambda}{60}\cos^{-1}\left(\frac{2}{\sqrt{\cos \Lambda} + 1.992} + 0.0439\right)\right]\right\}$$

Equations (4) and (5) are derived for cases where $k \approx w$, and spacing between grit elements is defined by the equation

$$s = \frac{4k}{\cos \Lambda}$$

For the present model ($\Lambda = 55^o$, $S = 0.2045\ m^2$, $\ell = 243.7$ cm), equations (4) and (5) reduce to the following simplified equations:

$$\Delta C_D = (0.00265 - 0.00010M_\infty)\frac{k^2}{\delta^*_k} \qquad \left(\frac{k}{\delta^*_k} \leq 5\right) \tag{6}$$

and

$$\Delta C_D = (0.0133 - 0.0005M_\infty)k \qquad \left(\frac{k}{\delta^*_k} > 5\right) \tag{7}$$

Calculated grit drag increments from equations (6) and (7) are compared with measurements from the present tests in figure 11. Since equations (6) and (7) only predict the increment in drag coefficient due to the transition strips, it is necessary to establish the grit-free turbulent drag level of the model and add to this value the predicted grit drag increments before comparisons can be made with the measured total drag values. In figure 11, the grit-free turbulent drag levels were approximated by fairing a straight line though the data points for $k/\delta^*_k \leq 5$ to the ordinate axis ($k^2 = 0\ cm^2$). In general, the predicted grit drag increments agree well with measurements for Mach 1.5 to 3.95 at $R = 1.15 \times 10^7\ m^{-1}$ (fig. 11(a)). Also, the few data points obtained for $k/\delta^*_k > 5$ indicate a change in slope in the $C_{D,o}$ curves in the vicinity of $k/\delta^*_k = 5$ as predicted. The predicted grit drag increments at $M_\infty = 4.63$ and $R = 1.15 \times 10^7\ m^{-1}$ are considerably less than those measured. For this Mach number and Reynolds number, $C_{D,o}$ measurements for the two largest roughness sizes only were used to determine the grit-free drag level. Even for these very large grits there is some doubt that the $k = 0.078$ cm grit induced fully turbulent flow at this Reynolds number. A small error

in $C_{D,o}$ for the $k = 0.078$ cm grit results in a large error when extrapolated to $k^2 = 0$ cm^2 to determine the grit-free drag level. If this lack of fully turbulent flow is the reason for poor agreement, then better agreement would be expected at the higher Reynolds numbers. To determine whether this is the case, predicted and measured grit drag increments are compared in figure 11(b) for $R = 1.64 \times 10^7$ m^{-1} and much better agreement is obtained. Therefore, the results presented in figure 11 suggest that the prediction method gives realistic estimates of grit drag increment for zero-lift conditions, at least for the range of test variables of this investigation.

The data of reference 14 indicate that if fully turbulent flow occurs over a model near zero lift, the drag increment due to roughness is relatively insensitive to changes in angle of attack or lift. To determine whether this phenomenon occurred for the test conditions of the present tests, the data were examined as shown in figure 12. Results are presented in the form of C_A in lieu of C_D since the drag due to lift of the present model results in very large drag coefficients at the larger angles of attack with corresponding insufficient data resolution to determine the magnitude of the grit drag. Also, for the maximum angles of attack of the present tests, C_A and C_D for the roughness elements differ by only approximately 5 percent. The results shown in figure 12 indicate that the grit drag increment remains approximately constant for the test range of angle of attack. Limited thin-film data obtained at $R = 1.312 \times 10^7$ m^{-1} and $M_\infty = 4.63$ indicate that at the larger angles of attack, large regions of laminar flow occurred on the model leeward surface for the smaller roughness elements similar to the results shown in figure 8(a). This increase in extent of laminar flow would be expected to reduce the skin-friction drag which then results in an increase at the larger angles of attack in the difference between C_A values for the smaller roughness elements and the larger roughness elements. The constant increment in C_A for the different roughness sizes through the range of angles of attack shown in figure 12 indicates this anticipated increase did not occur. This lack in sensitivity of the axial-force measurements to the increase in extent of laminar flow over the leeward surface possibly results from the fact that the skin-friction drag over the model windward surface (flow over which is fully turbulent as indicated by the thin-film data) is much larger than that which occurs on the leeward surface. The windward turbulent friction drag apparently dominates the total friction drag. Preliminary estimates based on two-dimensional considerations indicate that the friction drag on the windward surface of the present model at $\alpha \approx 16^\circ$ and Mach 4.63 is over an order of magnitude greater than that which occurs on the leeward surface for fully turbulent conditions.

The effects of grit size on measured aerodynamic characteristics of the present model are shown in figure 13 for the minimum and maximum Mach numbers of the investigation at $R = 6.56 \times 10^6$ m^{-1}. In general, these results show that grit size had

little or no effect on C_L and C_m. For angles of attack ranging from 0^o to values corresponding to maximum L/D, increasing grit size results in an increase in C_D and a decrease in L/D, as would be expected. These grit effects result from the increase in grit wave drag with increasing k and in some cases to the increase in extent of turbulent flow with increasing k. The results shown in figure 13 indicate that the consequence of using large roughness elements depends on the particular aerodynamic characteristic parameter of interest. For example, if C_L and C_m are of primary concern, then roughness size is of little importance; whereas if C_D and L/D are the principal measurements, then the effects of roughness size must be taken into consideration. Also, as previously discussed, the difficulty associated with obtaining a fully turbulent condition on the model leeward surface at angles of attack could significantly alter separation characteristics ahead of control surfaces. This effect must be considered if measurements such as control effectiveness are of primary interest. The model used in the present investigation did not have movable control surfaces and, therefore, control effectiveness measurements were not obtained.

SUMMARY OF RESULTS

An experimental investigation has been conducted to determine the effects of roughness size on the position of boundary-layer transition and on the aerodynamic characteristics of a 55^o swept-delta-wing model. The tests were conducted at free-stream Mach numbers from 1.5 to 4.63, Reynolds numbers per meter from 3.3×10^6 to 1.6×10^7, angles of attack from -8^o to 16^o, and roughness sizes ranging from 0.027-cm sand grit to 0.127-cm-high cylinders. The results are summarized as follows:

1. Near 0^o angle of attack, effective roughness Reynolds numbers for the model used in this investigation were generally less than existing flat-plate data.

2. Within the frequency range of the thin-film gauge instrumentation used in the present test ($\approx$15 kHz), roughness size had little effect on turbulence level at the model surface once fully turbulent flow was established.

3. Increasing angle of attack resulted in transition moving downstream on the model leeward surface and moving upstream on the model windward surface. At Mach 4.63 and angle of attack of approximately 16^o, large regions of laminar flow occurred on the model leeward surface for all roughness sizes tested.

4. Results from empirical equations, derived from the data of NASA Technical Notes D-7369 and D-7812, for predicting the drag of roughness elements used in boundary-layer trips are in good agreement with measurements from the present tests.

5. Experimental data from the present tests indicate grit drag increment remains approximately constant with changes in angle of attack up to the maximum angles tested.

6. For the full range of test variables, grit size had little or no effect on lift coefficient and pitching moment. Significant effects of grit size were observed on drag coefficient and lift-drag ratio.

Langley Research Center
National Aeronautics and Space Administration
Hampton, VA 23665
October 26, 1977

APPENDIX

DRAG PREDICTION OF BOUNDARY-LAYER TRIPS

Described in this appendix is a method to predict the drag of roughness elements used for boundary-layer trips based on the data of references 4 and 5. Although the data of references 4 and 5 are for small circular cylinders, it is assumed in this paper that the data are equally applicable to sand grit elements.

In order to simplify the present method, the cylinder results from references 4 and 5 were converted to the parameter $C_{D,C}/C_{D,IC}$ and were used to empirically derive the following equation:

$$\frac{C_{D,C}}{C_{D,IC}} = \left[1 - \frac{w}{s}(0.191 + 0.172M_\infty) - \left(\frac{w}{s}\right)^2(0.545 + 0.491M_\infty)\right] \times \left\{\cos\left[\frac{\Lambda}{60}\cos^{-1}\left(\frac{1}{\sqrt{\frac{w}{s}} + 0.996} + 0.0439\right)\right]\right\} \tag{A1}$$

Data from reference 5 are compared with calculations from equation (A1) in figure 14 for Mach 2.30 to Mach 4.60 and sweep angles from 0° to 60°. Good agreement is shown for this range of variables.

In order to approximate $C_{D,IC}$, the results of reference 4 for the case of a cylinder having equal height and diameter were approximated by the equations

$$C_{D,IC} = 0.2\frac{k}{\delta^*_k} \qquad \left(\frac{k}{\delta^*_k} \leq 5\right) \tag{A2}$$

and

$$C_{D,IC} = 1.0 \qquad \left(\frac{k}{\delta^*_k} > 5\right) \tag{A3}$$

and as shown in figure 15 these approximations are in general agreement with the experimental data. For the cylindrical elements of the present tests $k = w$, and although the sand elements were of random shapes, it is believed that this equality is also approximated for the average element.

APPENDIX

The roughness element drag coefficient is obtained from equations (A1), (A2), and (A3) combined with the equation

$$C_{D,C} = \frac{C_{D,C}}{C_{D,IC}} C_{D,IC} \tag{A4}$$

The total drag force for all elements in the transition strip can be approximated from the equation

$$\text{Drag force} = C_{D,C} q_\infty A_c N \tag{A5}$$

where A_c is the projected frontal area of a typical element and N is the total number of elements.

The increment in model drag coefficient due to roughness drag is calculated from the equation

$$\Delta C_D = \frac{\text{Roughness drag force}}{q_\infty S} \tag{A6}$$

which when combined with equations (A2), (A3), (A4), and (A5) gives

$$\Delta C_D = 0.2N \frac{A_c}{S} \frac{k}{\delta^*_k} \frac{C_{D,C}}{C_{D,IC}} \qquad \left(\frac{k}{\delta^*_k} \leqq 5\right) \tag{A7}$$

and

$$\Delta C_D = N \frac{A_c}{S} \frac{C_{D,C}}{C_{D,IC}} \qquad \left(\frac{k}{\delta^*_k} > 5\right) \tag{A8}$$

where from equation (A1)

$$\frac{C_{D,C}}{C_{D,IC}} = f\left(\Lambda, M_\infty, \frac{w}{s}\right)$$

Since it was previously assumed that

$$k = w$$

then

$$A_c = 0.0001k^2 \tag{A9}$$

Also

$$N = \frac{l}{s} \tag{A10}$$

where l is the total length of the transition strip and s is the spacing between elements from center to center. Customarily in many supersonic wind tunnels, grit spacing is determined from the equation

$$s = \frac{4k}{\cos \Lambda}$$

which when substituted into equation (A10) gives

$$N = \frac{l}{4k} \cos \Lambda \tag{A11}$$

Substituting equations (A9) and (A11) into equations (A7) and (A8) results in the following equations for grit drag increment:

$$\Delta C_D = (0.000005) \frac{l}{S} \frac{k^2}{\delta^*_k} g(\Lambda, M_\infty) \qquad \left(\frac{k}{\delta^*_k} \leq 5 \right) \tag{A12}$$

and

$$\Delta C_D = (0.000025) \frac{l}{S} k \; g(\Lambda, M_\infty) \qquad \left(\frac{k}{\delta^*_k} > 5 \right) \tag{A13}$$

where

$$g(\Lambda, M_\infty) = (\cos \Lambda) \left[1 - (0.0478 + 0.0430 M_\infty) \cos \Lambda - (0.0341 + 0.0307 M_\infty) \cos^2 \Lambda \right]$$

$$\times \left\{ \cos \left[\frac{\Lambda}{60} \cos^{-1} \left(\frac{2}{\sqrt{\cos \Lambda} + 1.992} + 0.0439 \right) \right] \right\}$$

APPENDIX

It is important to note the variation of grit drag increment with k indicated by equations (A12) and (A13) when all other variables are held constant. For $k/\delta^*_k \leq 5$, equation (A12) indicates ΔC_D varies as k^2; whereas for $k/\delta^*_k > 5$, equation (A13) indicates ΔC_D varies linearly with k. This discontinuity in the variation of ΔC_D with k has been observed from experimental data obtained by other investigators. Figure 12 of reference 2 provides a good example. The discontinuity in slope of the reference 2 data occurs at $k \approx 5\delta^*_k$, and for $k < 5\delta^*_k$, ΔC_D varies as k^2 which is consistent with predicted trends of the present method.

Applying equations (A12) and (A13) to the model used in the present tests where

$\Lambda = 55^o$

$S = 0.2045\ m^2$

$\ell = 243.7\ cm$

results in the following simplified equations

$$\Delta C_D = (0.00265 - 0.0001M_\infty)\frac{k^2}{\delta^*_k} \qquad \left(\frac{k}{\delta^*_k} \leq 5\right) \tag{A14}$$

and

$$\Delta C_D = (0.0133 - 0.0005M_\infty)k \qquad \left(\frac{k}{\delta^*_k} > 5\right) \tag{A15}$$

where the units of both k and δ^*_k are cm.

REFERENCES

1. Dryden, Hugh L.: Review of Published Data on the Effect of Roughness on Transition From Laminar to Turbulent Flow. J. Aeronaut. Sci., vol. 20, no. 7, July 1953, pp. 477-482.

2. Braslow, Albert L.; Hicks, Raymond M.; and Harris, Roy V., Jr.: Use of Grit-Type Boundary-Layer-Transition Trips on Wind-Tunnel Models. NASA TN D-3579, 1966.

3. Morrisette, E. Leon; Stone, David R.; and Whitehead, Allen H., Jr.: Boundary-Layer Tripping With Emphasis on Hypersonic Flows. Viscous Drag Reduction, C. Sinclair Wells, ed., Plenum Press, 1969, pp. 33-51.

4. Stallings, Robert L., Jr.; Lamb, Milton; and Howell, Dorothy T.: Drag Characteristics of Circular Cylinders in a Laminar Boundary Layer at Supersonic Free-Stream Velocities. NASA TN D-7369, 1973.

5. Lamb, Milton; and Stallings, Robert L., Jr.: Sweep Effect on the Drag of Rows of Perpendicular Circular Cylinders in a Laminar Boundary Layer at Supersonic Free-Stream Velocities. NASA TN D-7812, 1974.

6. Sorrells, Russell B., III; and Landrum, Emma Jean: Theoretical and Experimental Study of Twisted and Cambered Delta Wings Designed for a Mach Number of 3.5. NASA TN D-8247, 1976.

7. Owen, F. K.: Transition Experiments on a Flat Plate at Subsonic and Supersonic Speeds. AIAA J., vol. 8, no. 3, Mar. 1970, pp. 518-523.

8. Cassels, William A.; and Campbell, James F.: Boundary-Layer Transition Study of Several Pointed Bodies of Revolution at Supersonic Speeds. NASA TN D-6063, 1970.

9. Manual for Users of the Unitary Plan Wind Tunnel Facilities of the National Advisory Committee for Aeronautics. NACA 1956.

10. Pate, S. R.; and Schueler, C. J.: Radiated Aerodynamic Noise Effects on Boundary-Layer Transition in Supersonic and Hypersonic Wind Tunnels. AIAA J., vol. 7, no. 3, Mar. 1969, pp. 450-457.

11. Potter, J. Leith; and Whitfield, Jack D.: Effects of Slight Nose Bluntness and Roughness on Boundary-Layer Transition in Supersonic Flows. J. Fluid Mech., vol. 12, pt. 4, Apr. 1962, pp. 501-535.

12. Potter, J. Leith; and Whitfield, Jack D.: Boundary-Layer Transition Under Hypersonic Conditions. Recent Developments in Boundary Layer Research, Part III, AGARDograph 97, May 1965, pp. 1-62.

13. Stainback, P. Calvin (with appendix by P. Calvin Stainback and Kathleen C. Wicker): Effect of Unit Reynolds Number, Nose Bluntness, Angle of Attack, and Roughness on Transition on a 5^{o} Half-Angle Cone at Mach 8. NASA TN D-4961, 1969.

14. Harris, Roy V., Jr.: Effects of Distributed Roughness Height on Aerodynamic Characteristics and Boundary-Layer Transition of a Wing-Body-Tail Configuration at a Mach Number of 1.61. NASA TN D-2334, 1964.

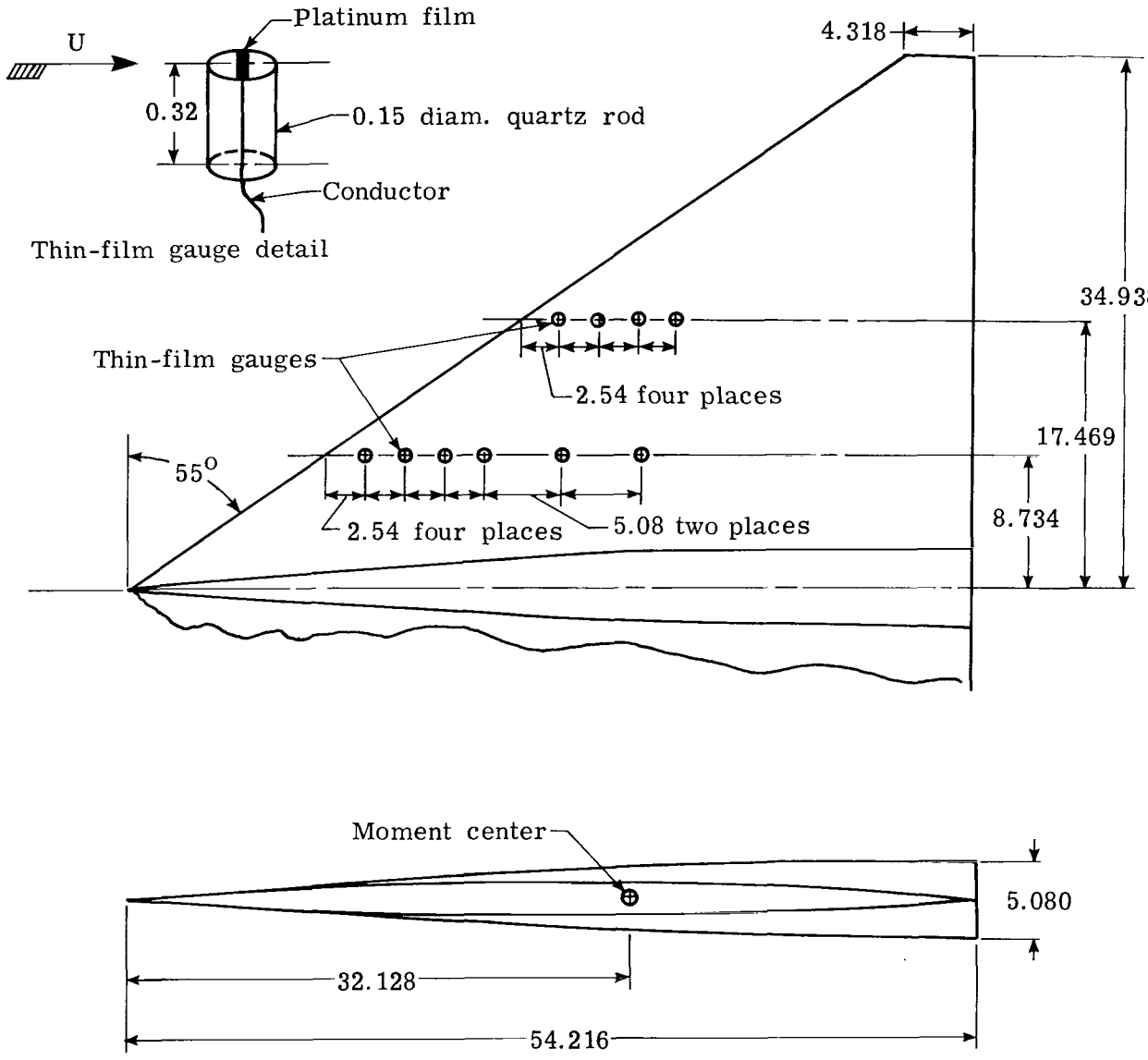

(a) Model geometry; all dimensions in cm.

Figure 1.- Model details.

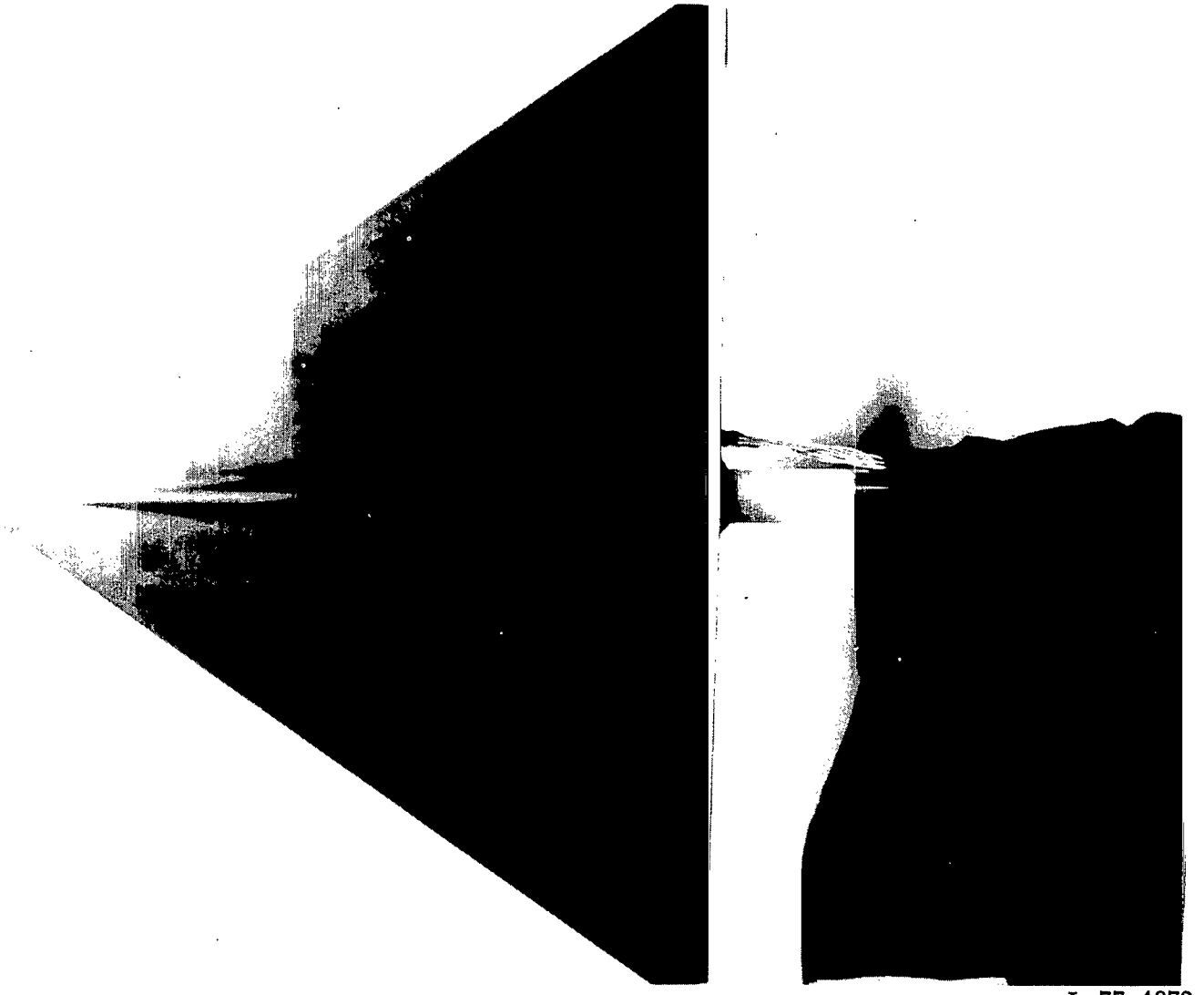

L-77-4872

(b) Photograph of model.

Figure 1.- Concluded.

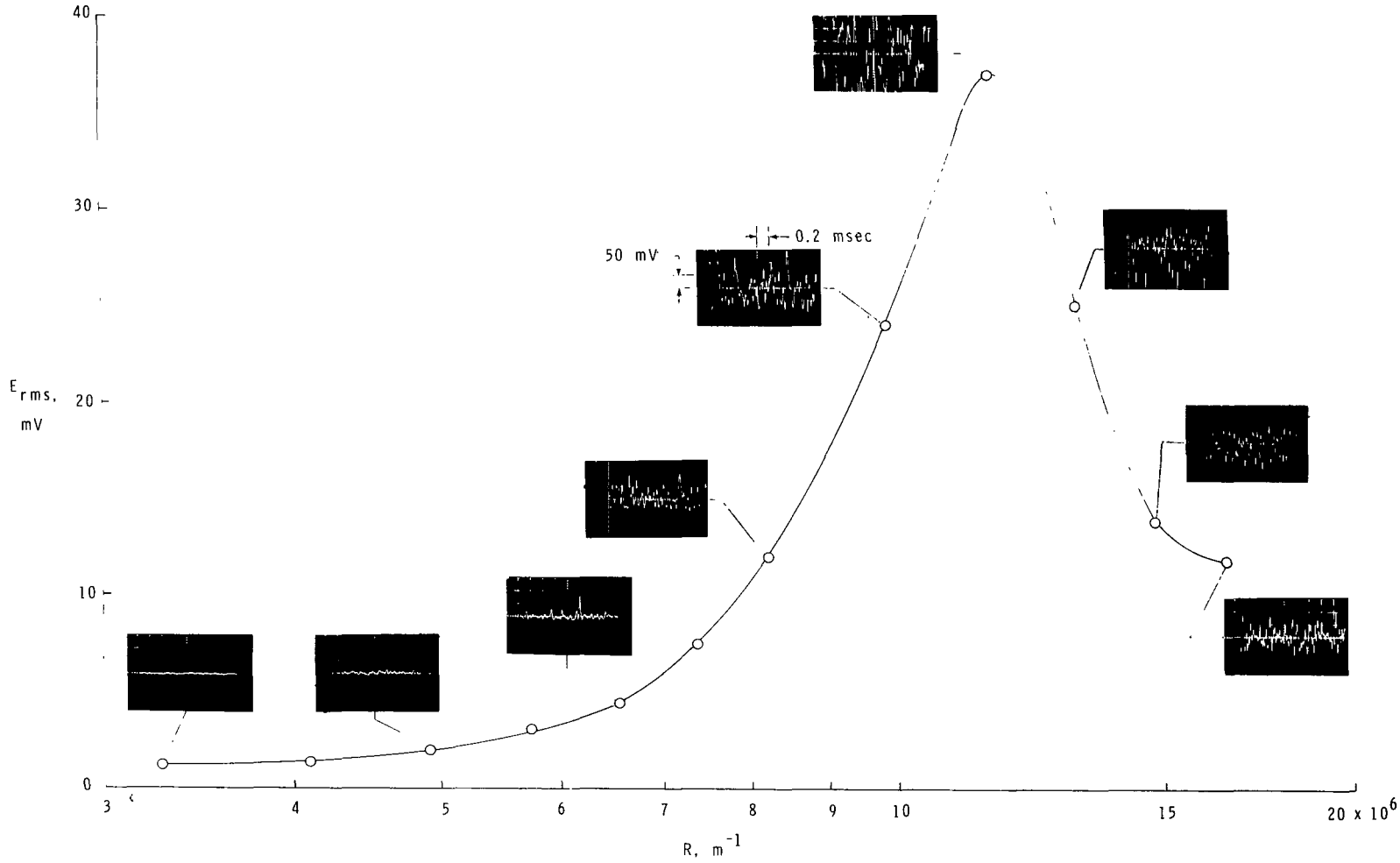

(a) Natural boundary-layer transition. x = 10.16 cm.

Figure 2.- Typical thin-film data. $M_\infty = 2.86$.

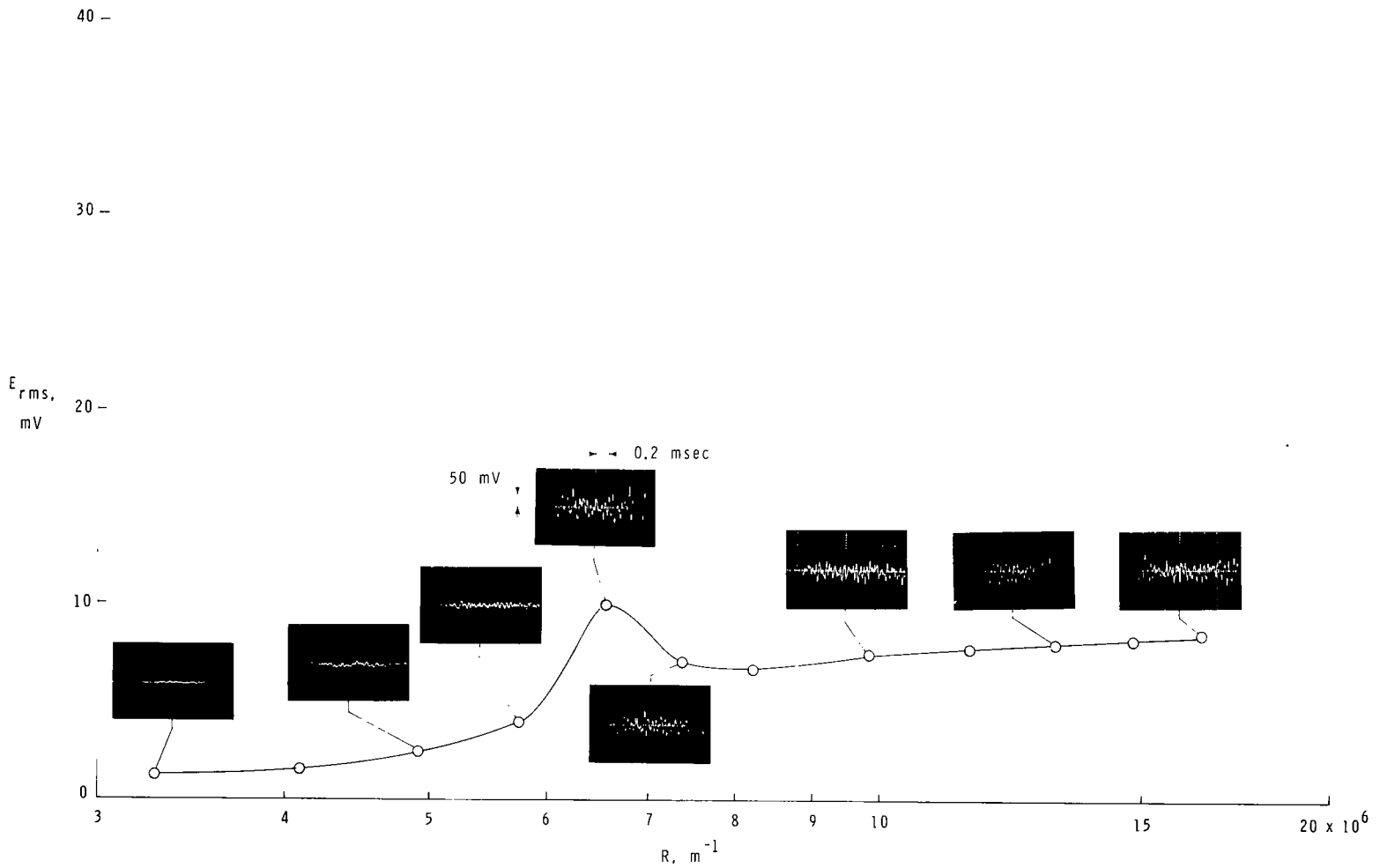

(b) Roughness-induced transition; k = 0.032 cm; x = 5.08 cm.

Figure 2.- Concluded.

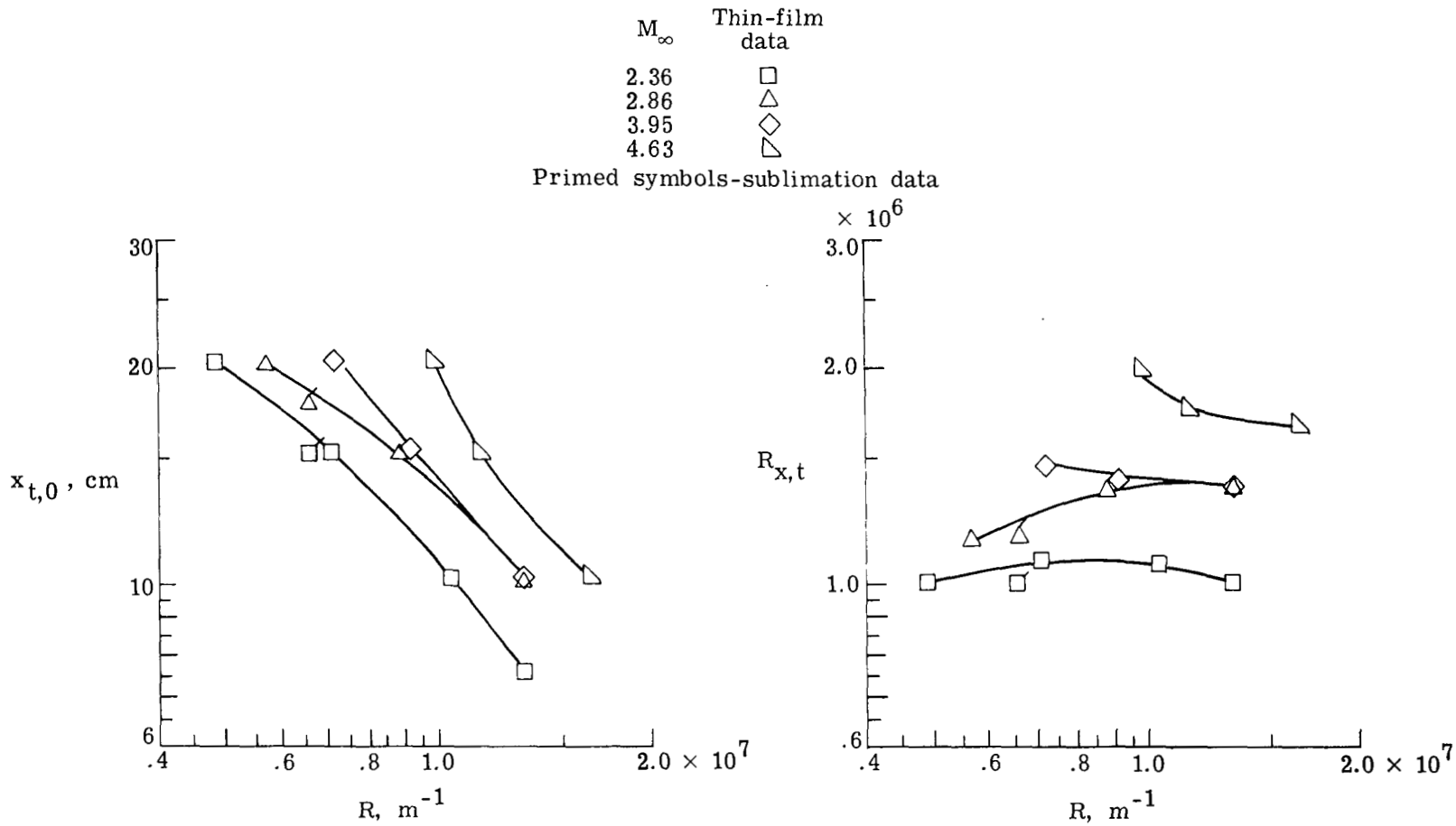

Figure 3.- Effect of unit Reynolds number on transition location and transition Reynolds number. k = 0 cm, $\alpha = 0^{o}$.

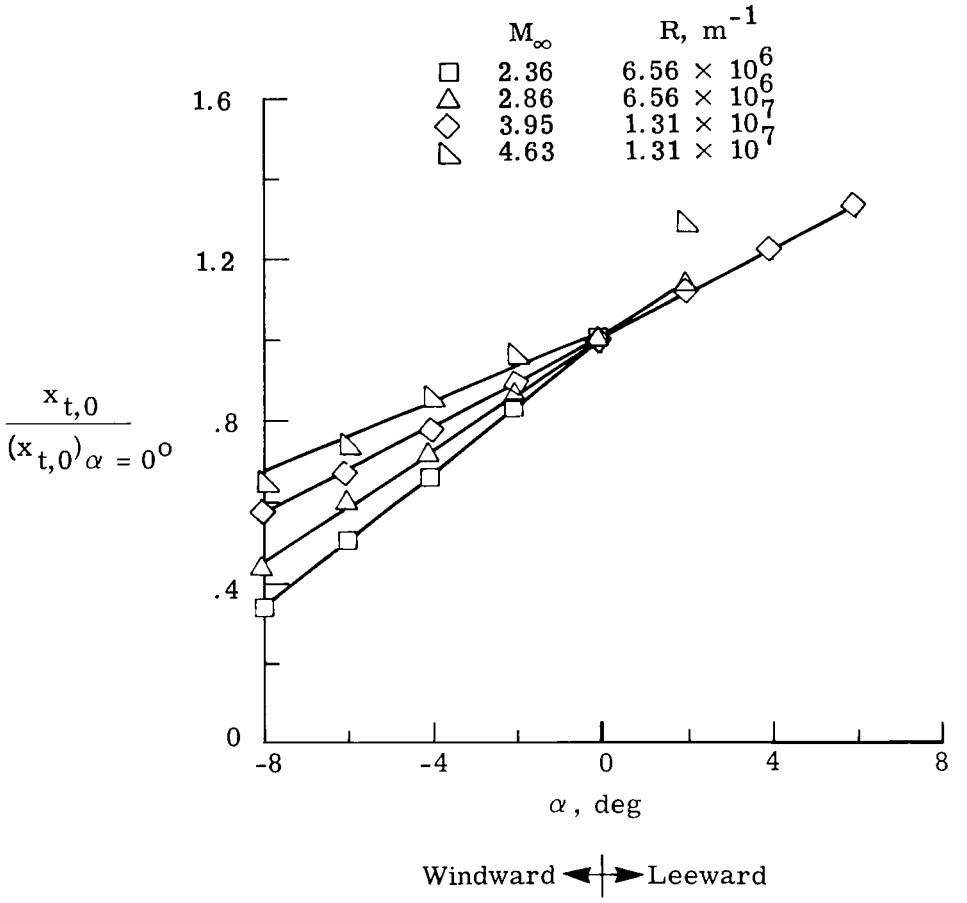

Figure 4.- Effect of angle of attack on transition location. k = 0 cm.

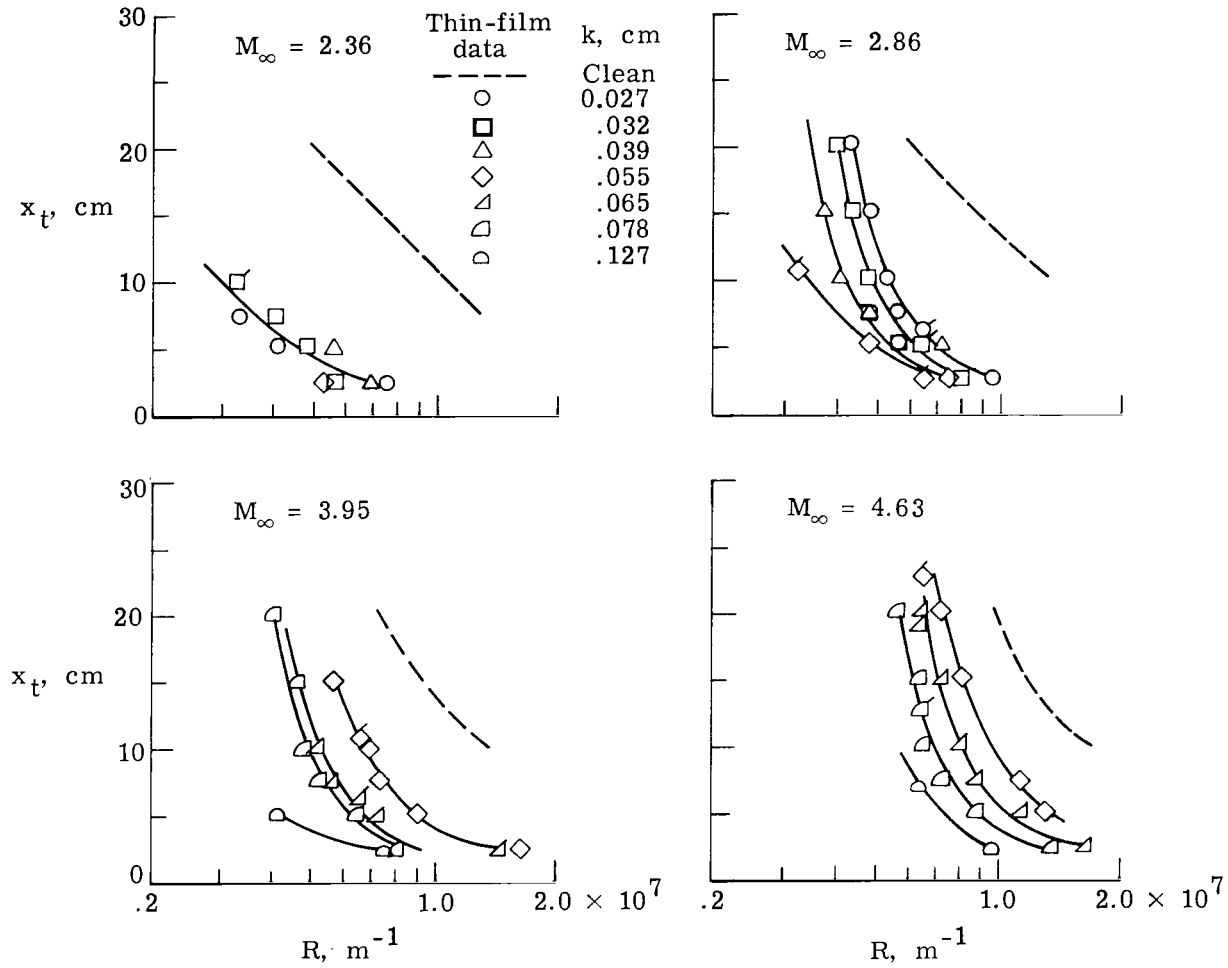

Figure 5.- Effect of k on transition location. $\alpha = 0^o$; primed symbols indicate sublimation data.

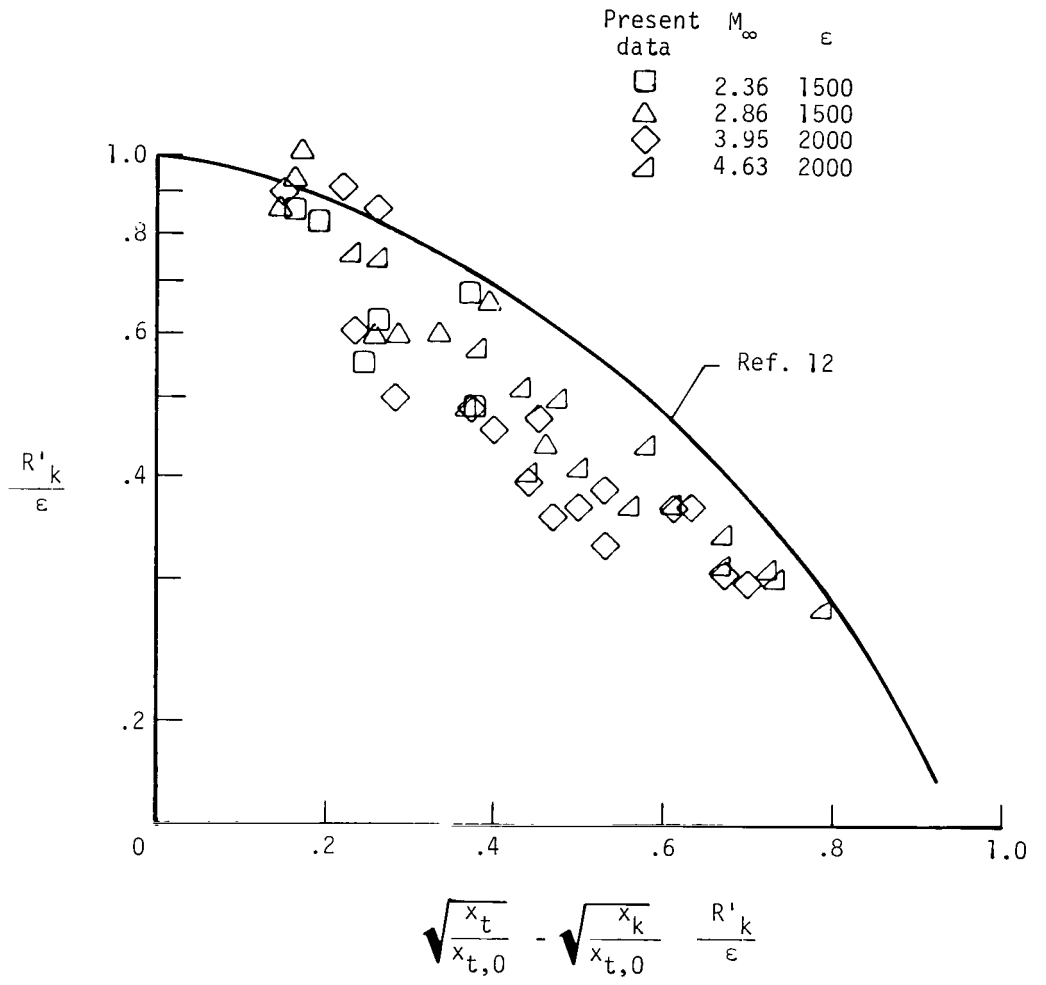

Figure 6.- Comparison of present data with hollow cylinder results from reference 11. Present data for $k \geq \delta_k$.

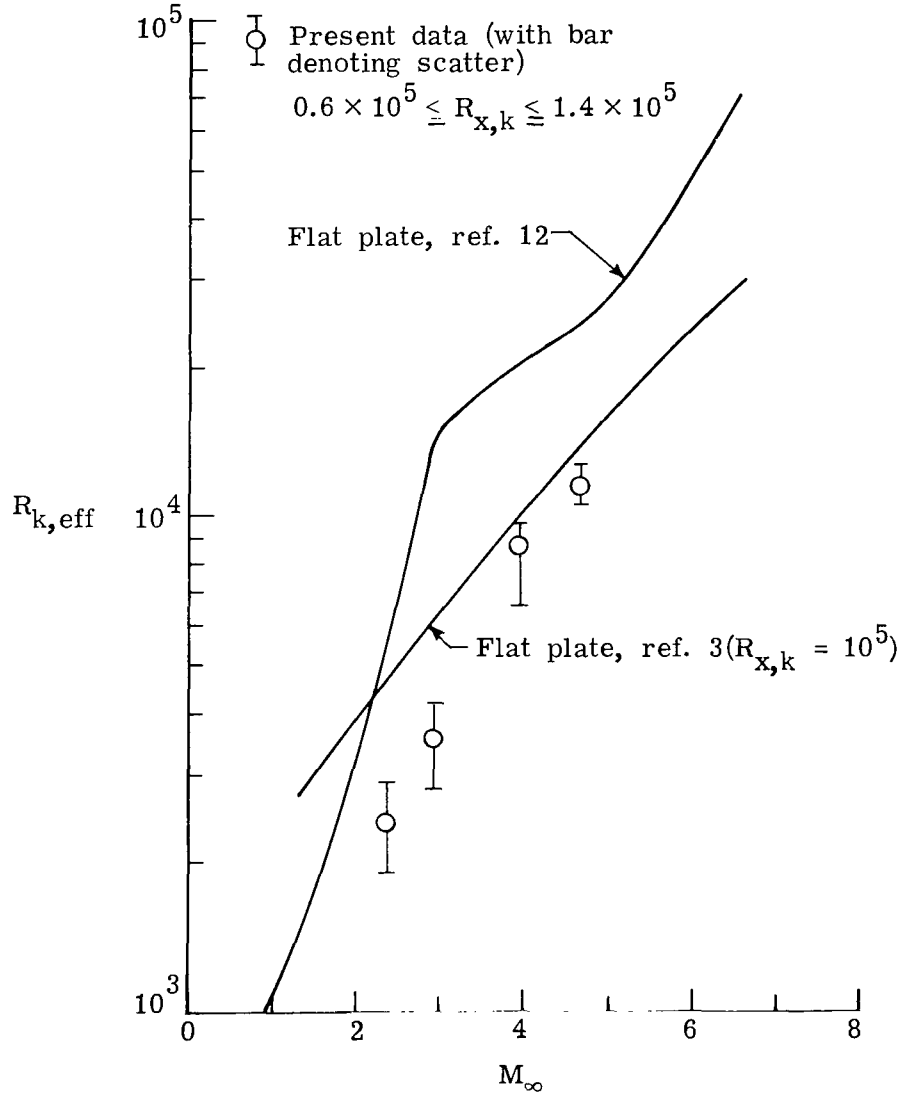

Figure 7.- Comparison of effective roughness Reynolds numbers from present tests with existing flat-plate data. $T_w = T_{aw}$; $\alpha = 0^o$; $k \geqq \delta_k$.

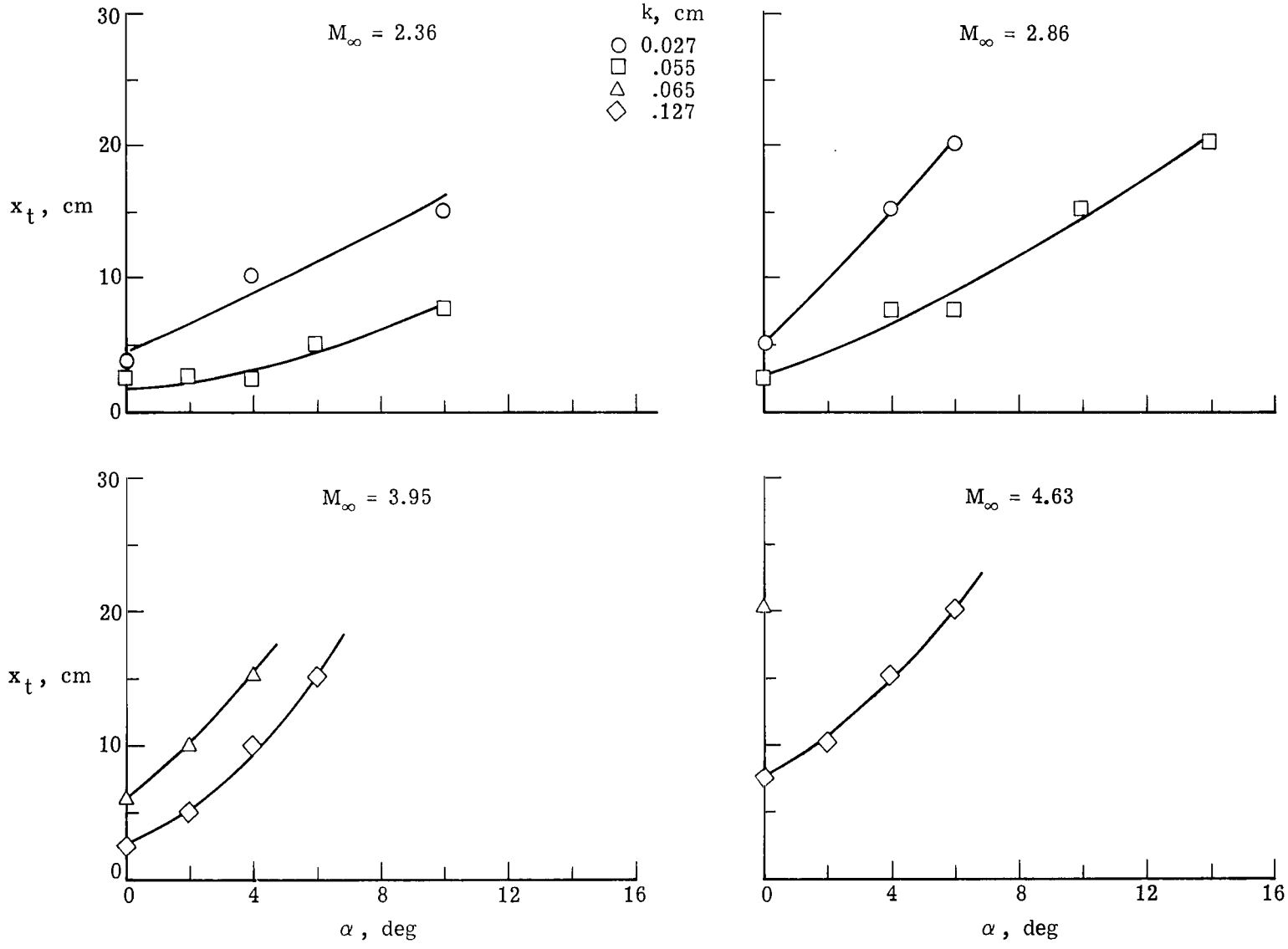

(a) Leeward side.

Figure 8.- Effect of angle of attack on transition location. $R = 6.56 \times 10^6\ m^{-1}$.

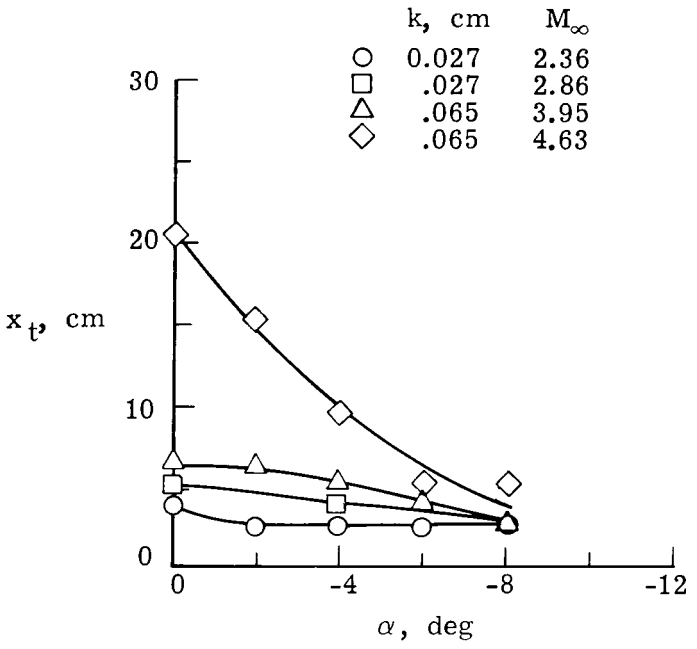

(b) Windward side.

Figure 8.- Concluded.

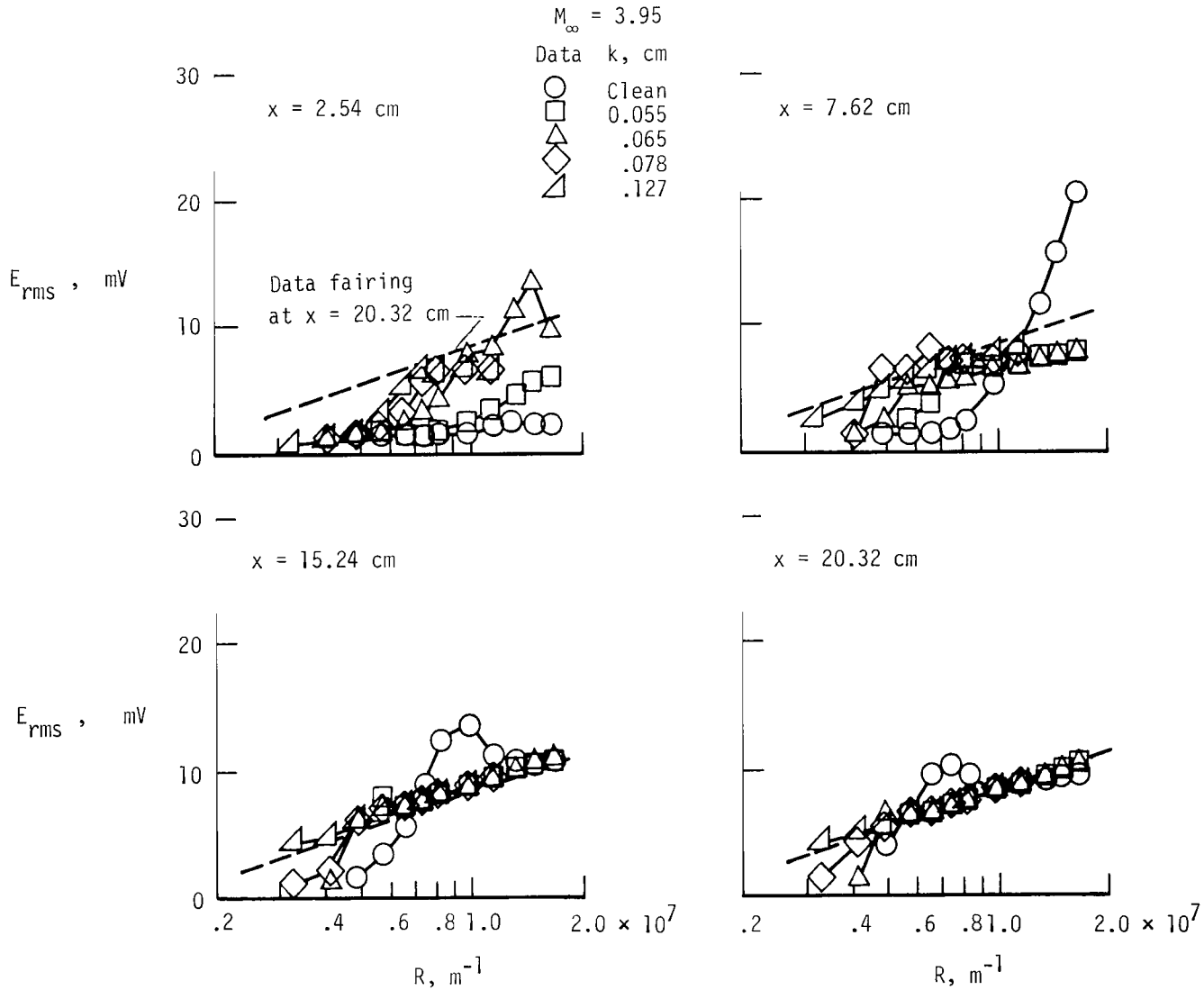

Figure 9.- Effect of k on thin-film gauge root-mean-square outputs.

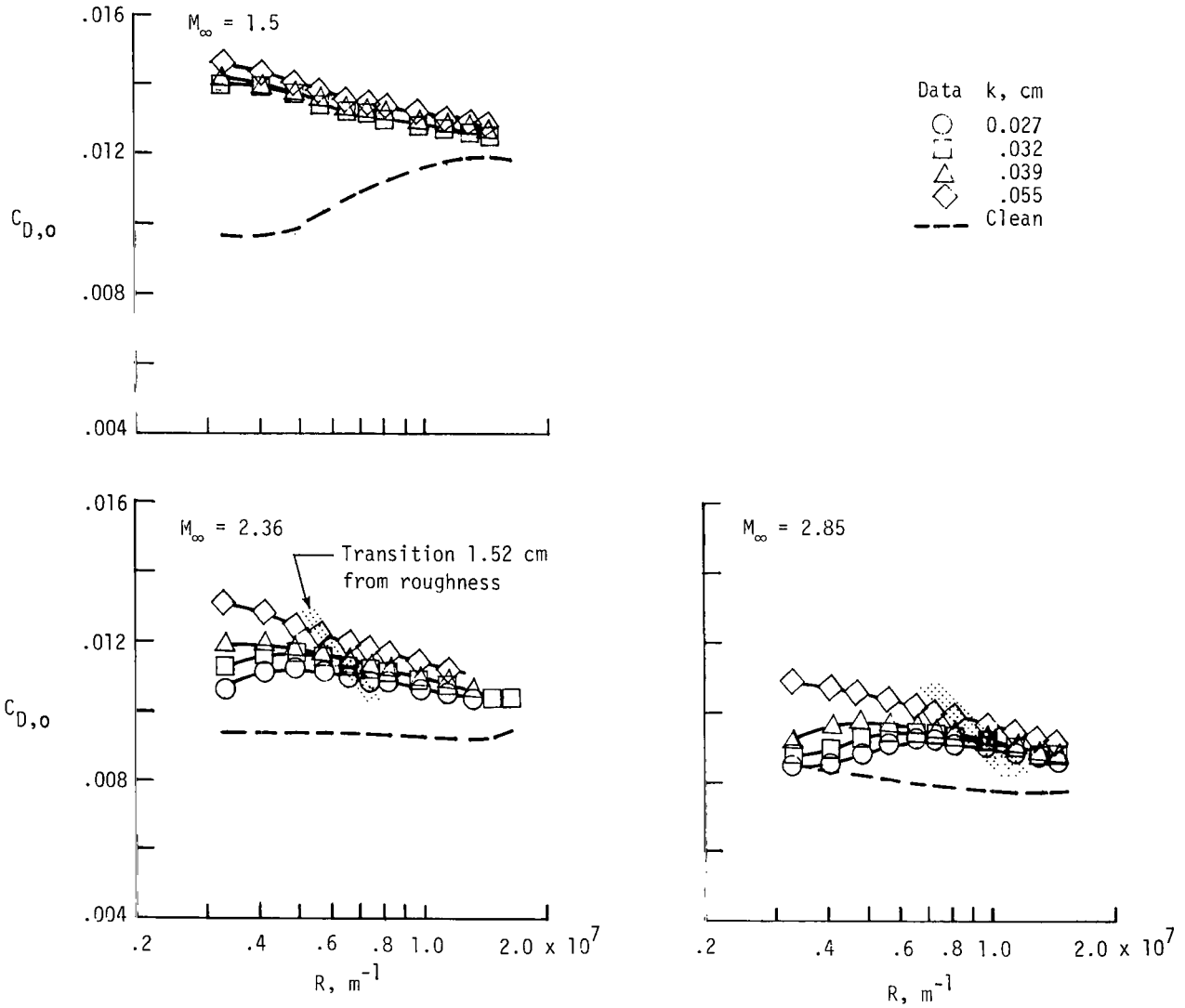

Figure 10.- Effect of k on drag at zero lift.

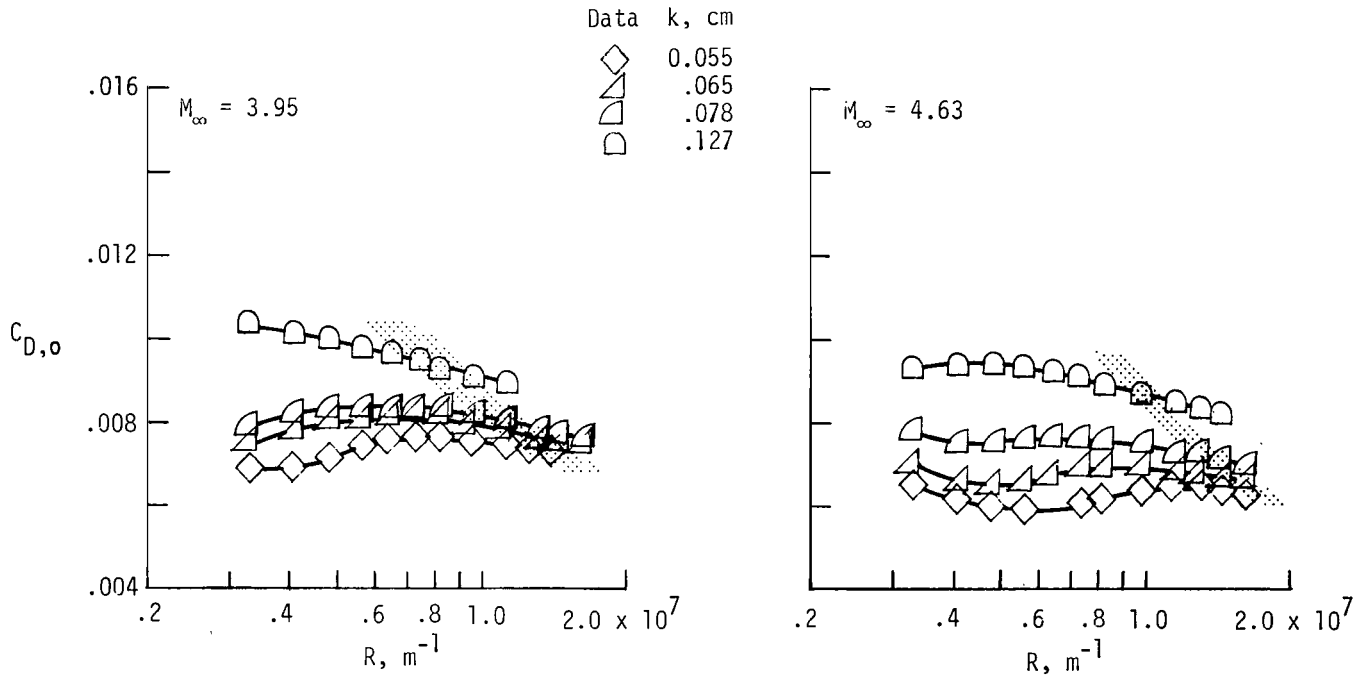

Figure 10.- Concluded.

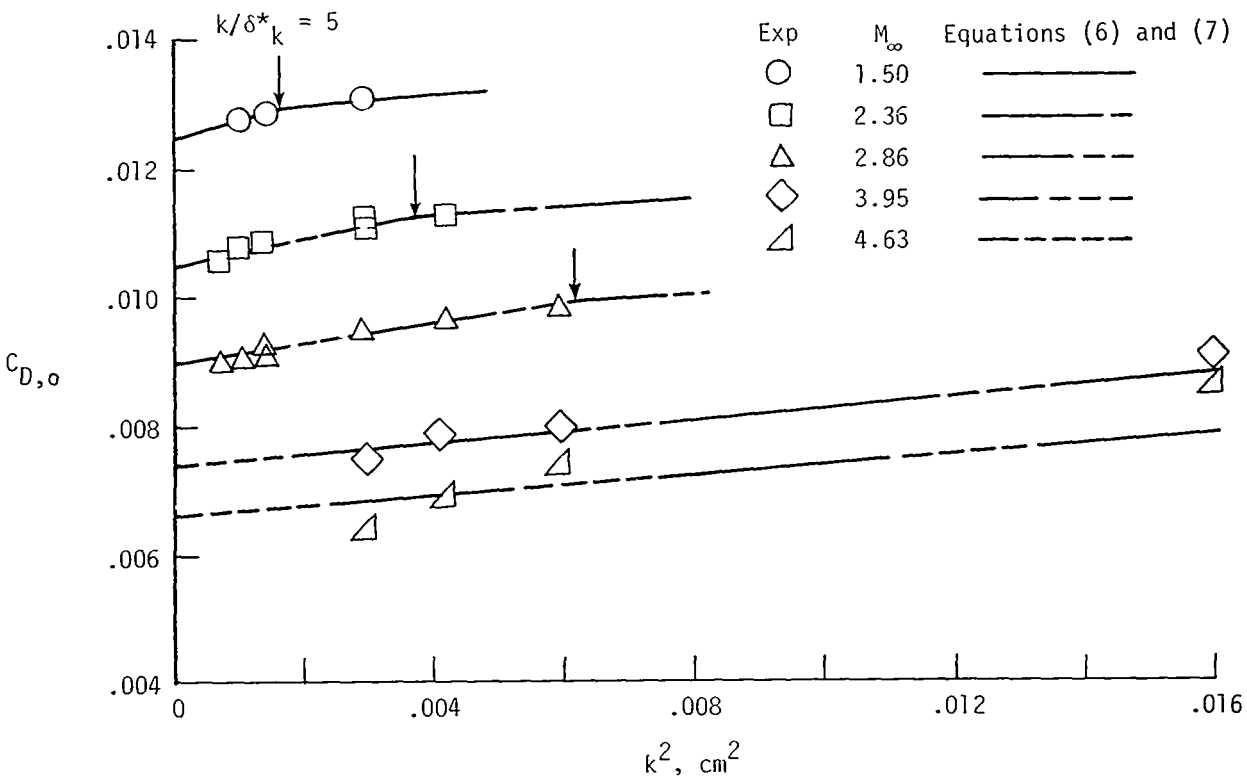

(a) $R = 1.15 \times 10^7\ m^{-1}$.

Figure 11.- Comparison of predicted grit drag with experiment. $\alpha = 0^o$.

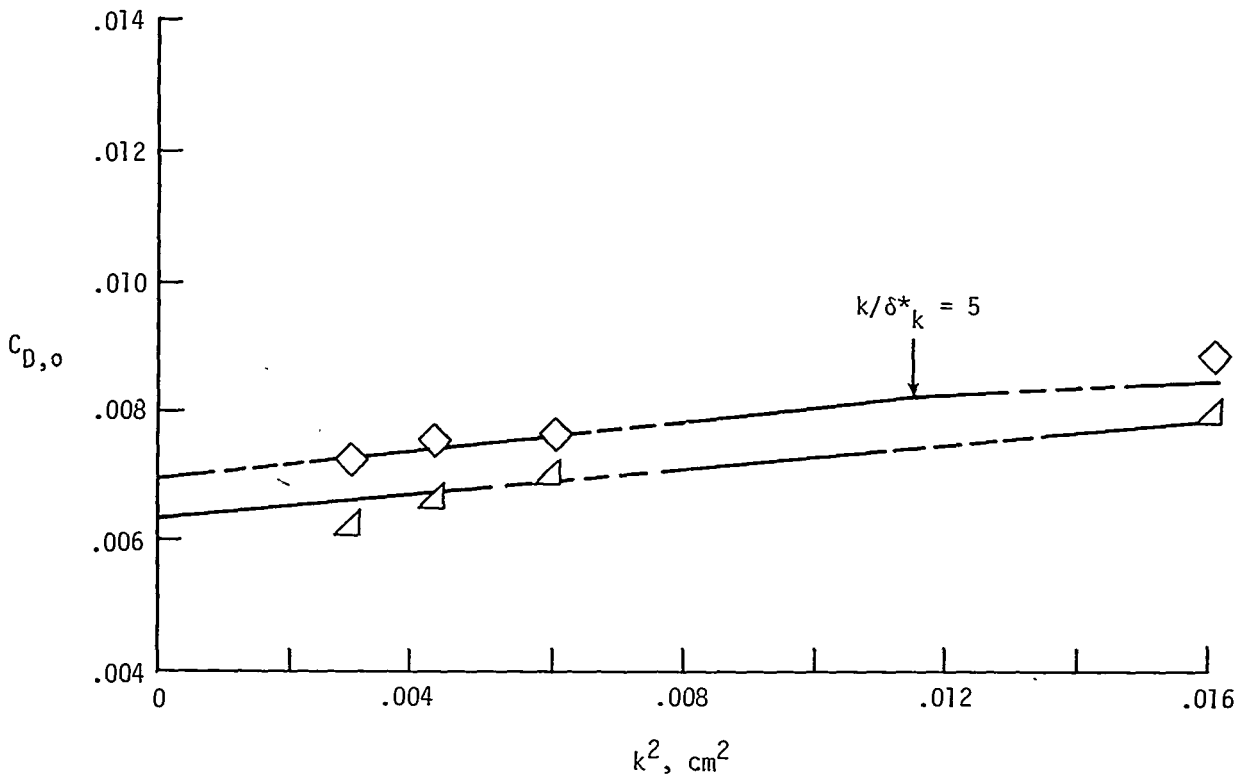

(b) $R = 1.64 \times 10^7\ m^{-1}$.

Figure 11.- Concluded.

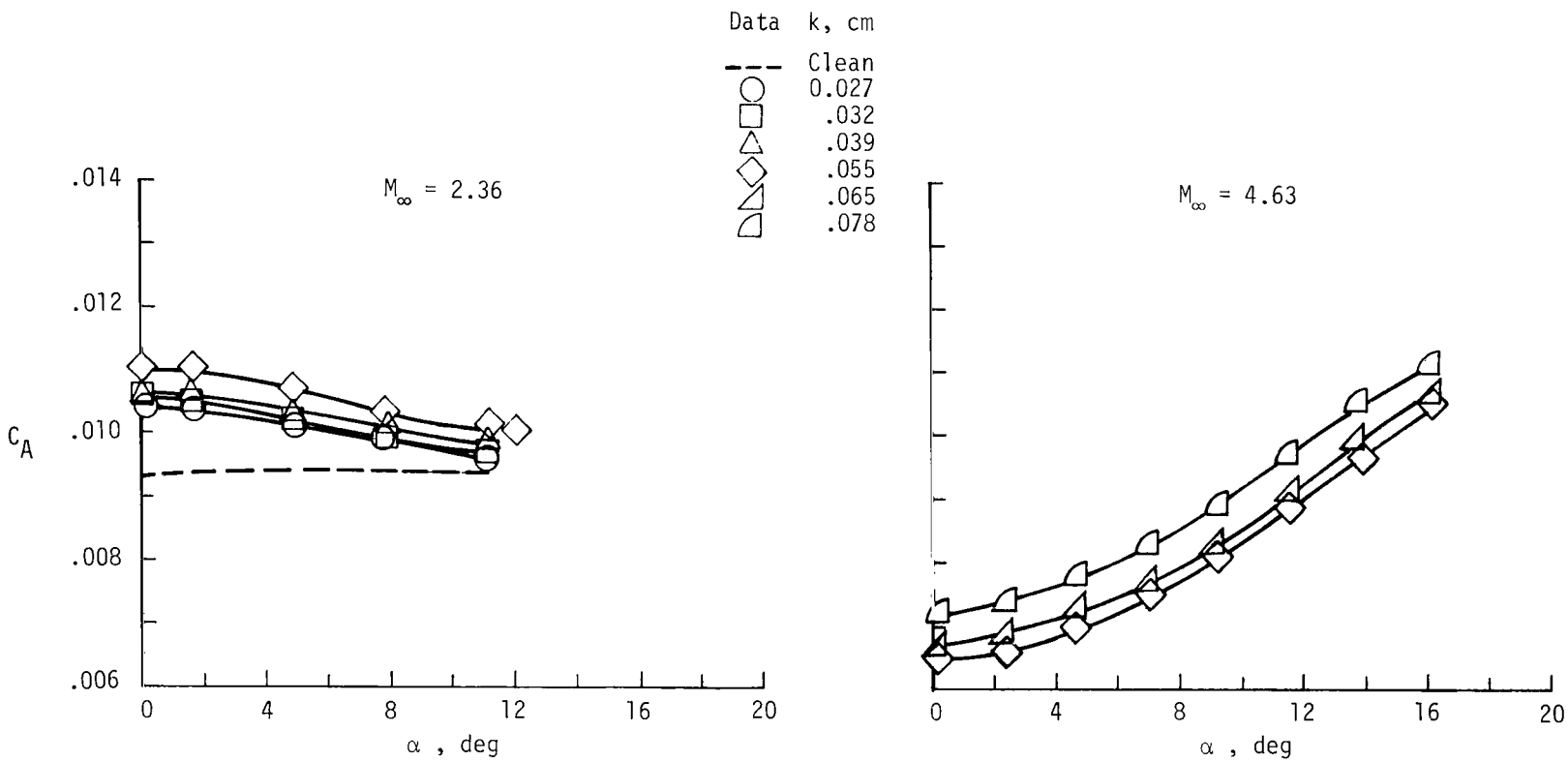

Figure 12.- Effect of angle of attack on experimental axial-force coefficients. $R = 1.312 \times 10^7\ m^{-1}$.

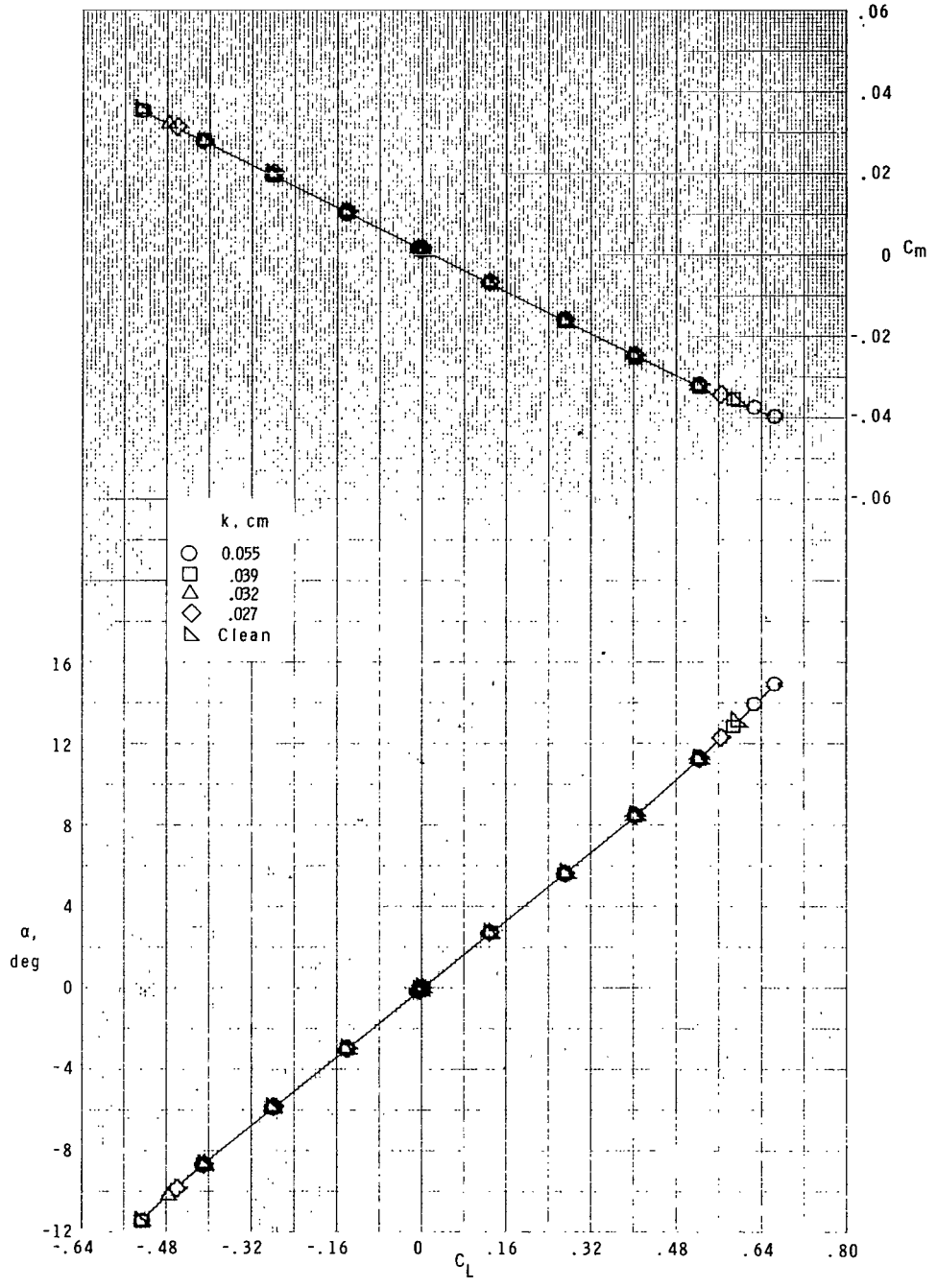

(a) $M_\infty = 1.5$.

Figure 13.- Effect of k on experimental aerodynamic forces and moments. $R = 6.56 \times 10^6\ m^{-1}$.

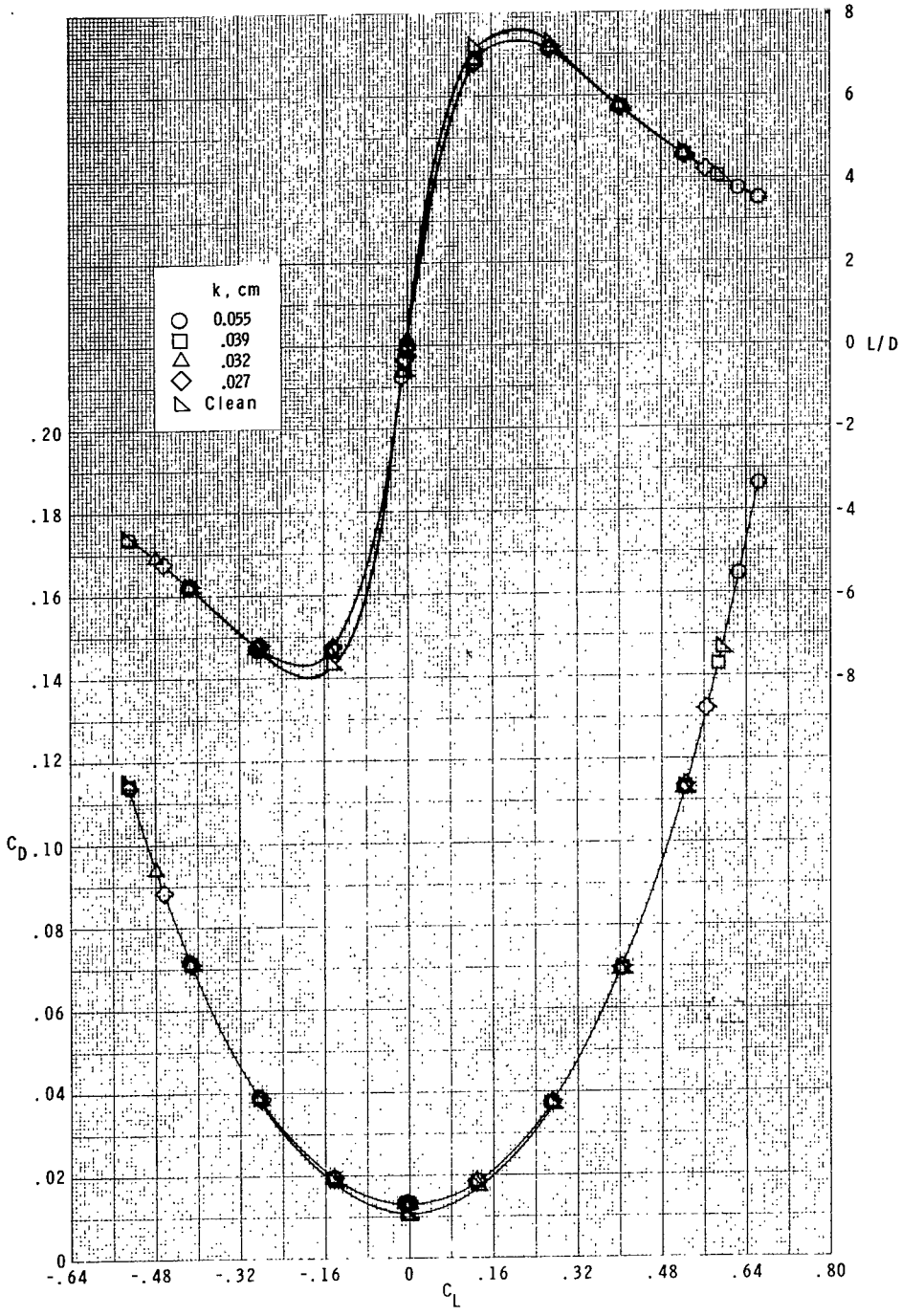

(a) Concluded.

Figure 13.- Continued.

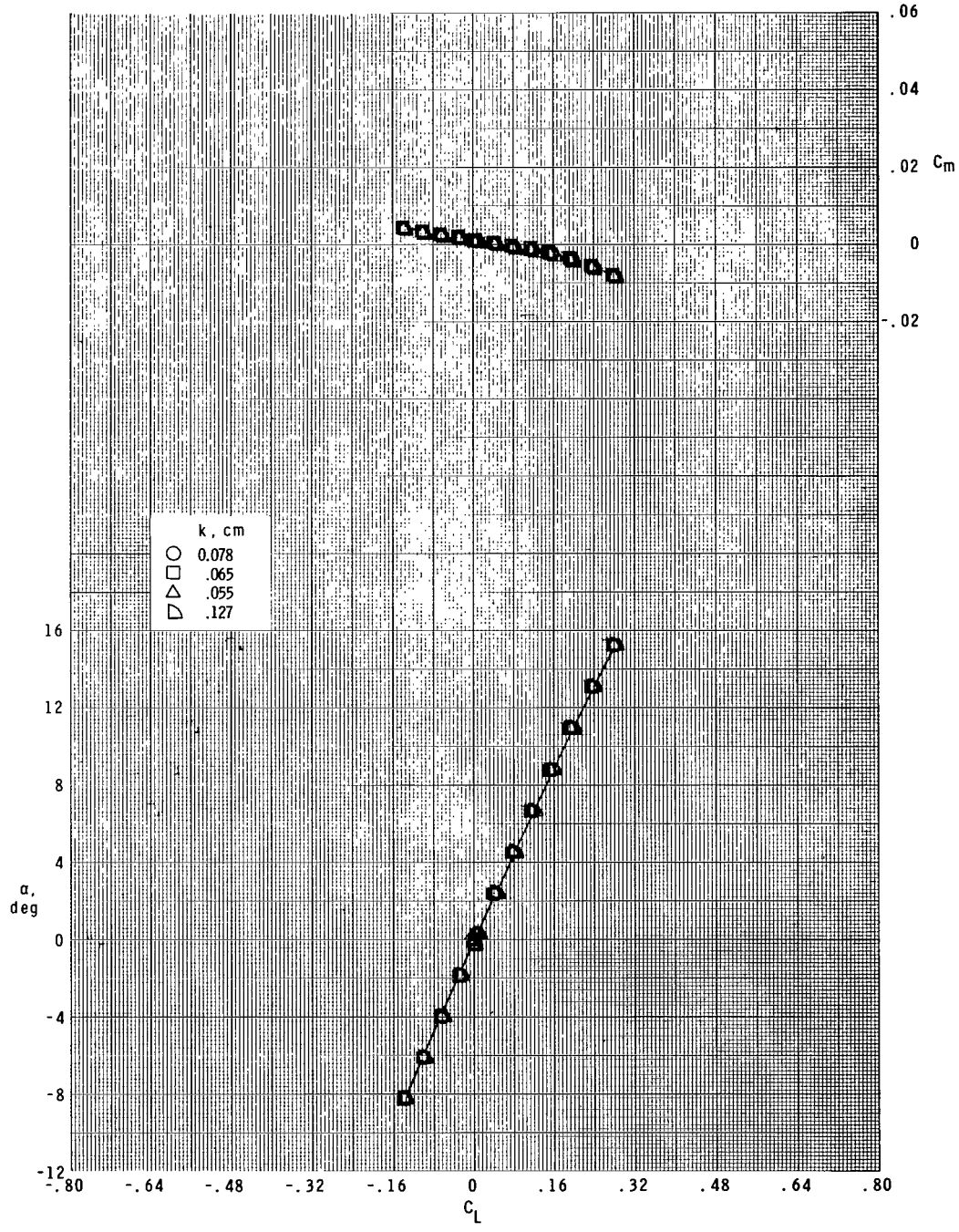

(b) $M_\infty = 4.63$.

Figure 13.- Continued.

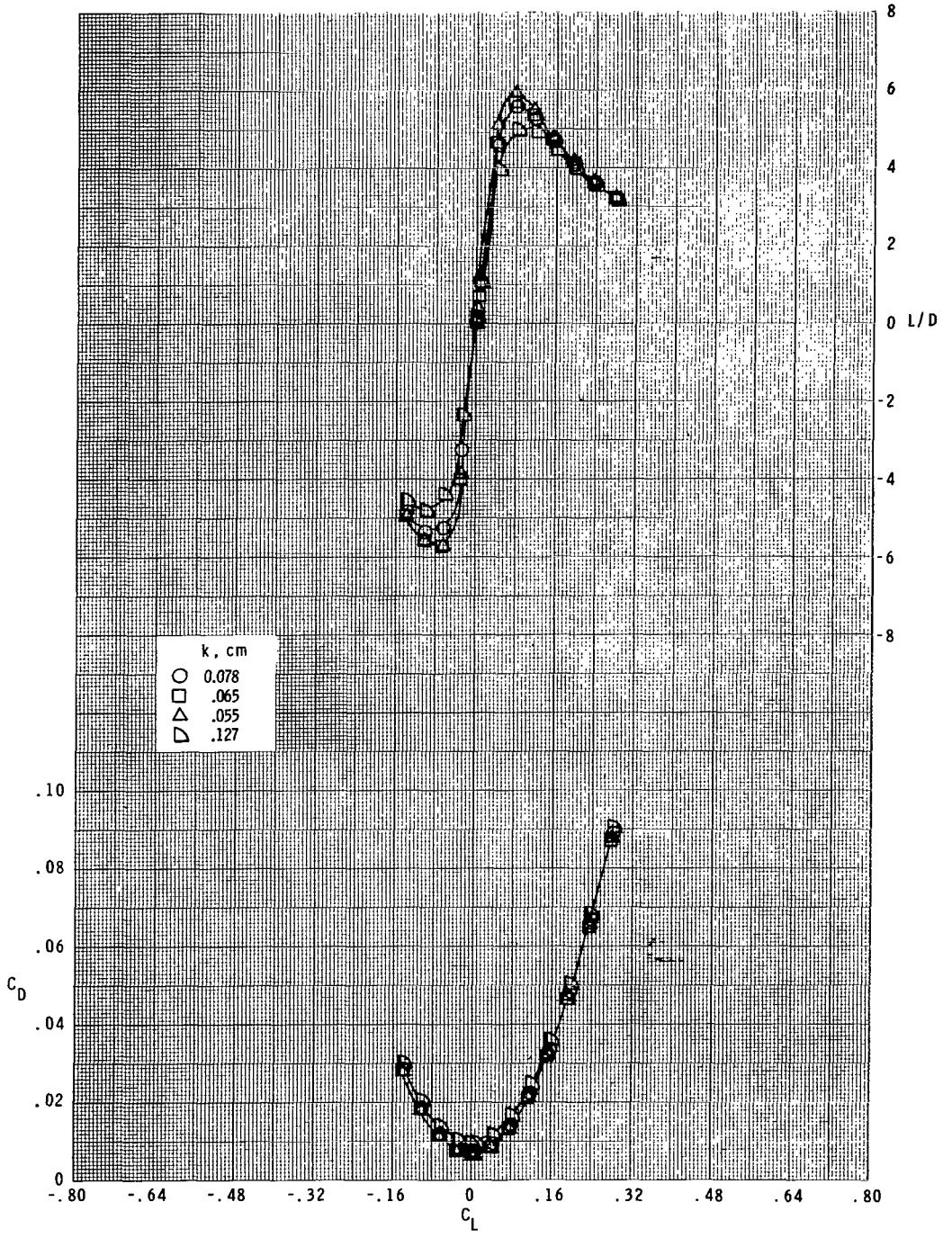

(b) Concluded.

Figure 13. - Concluded.

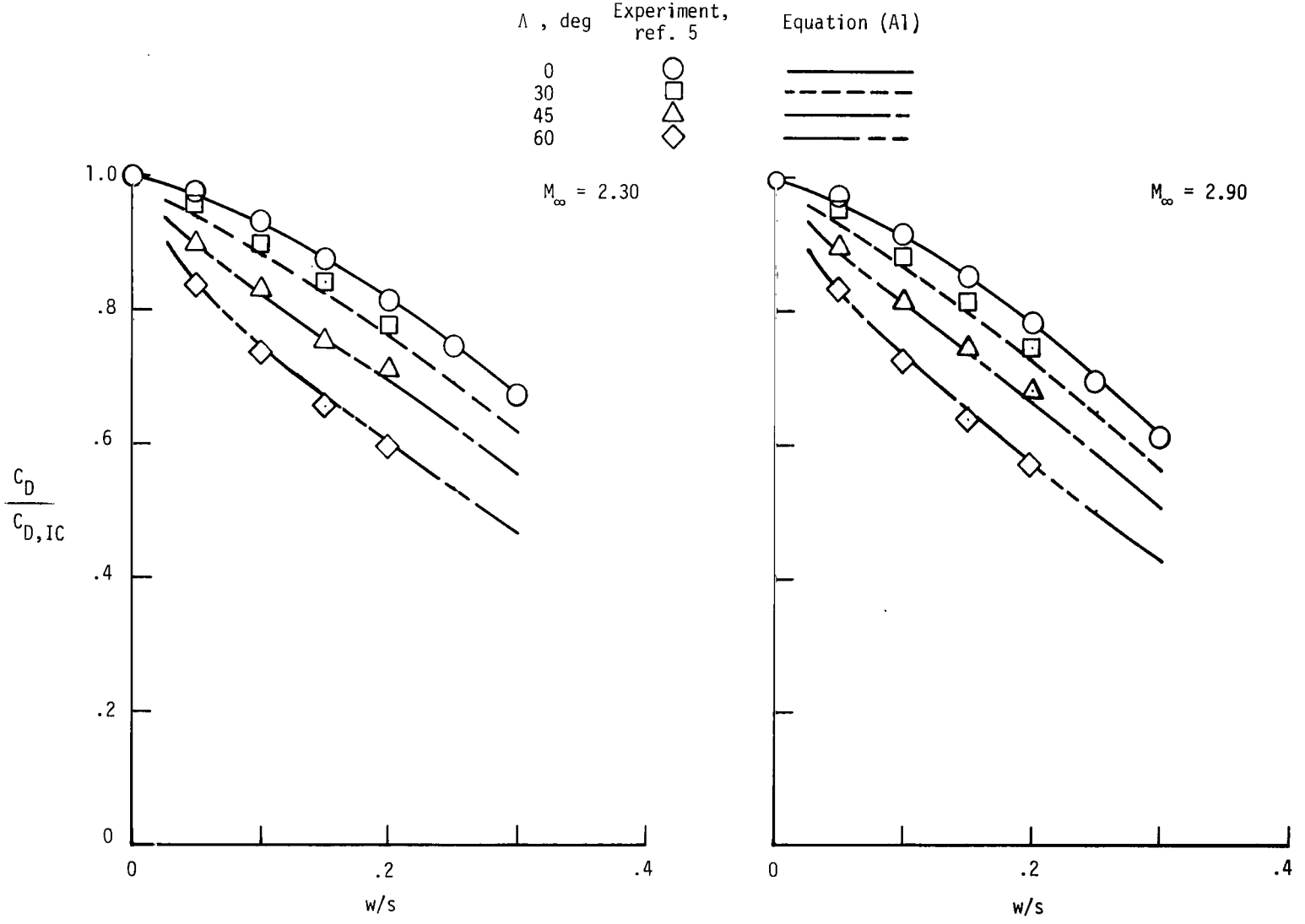

Figure 14.- Comparison of calculated and measured drag coefficients for circular cylinders used as boundary-layer trips.

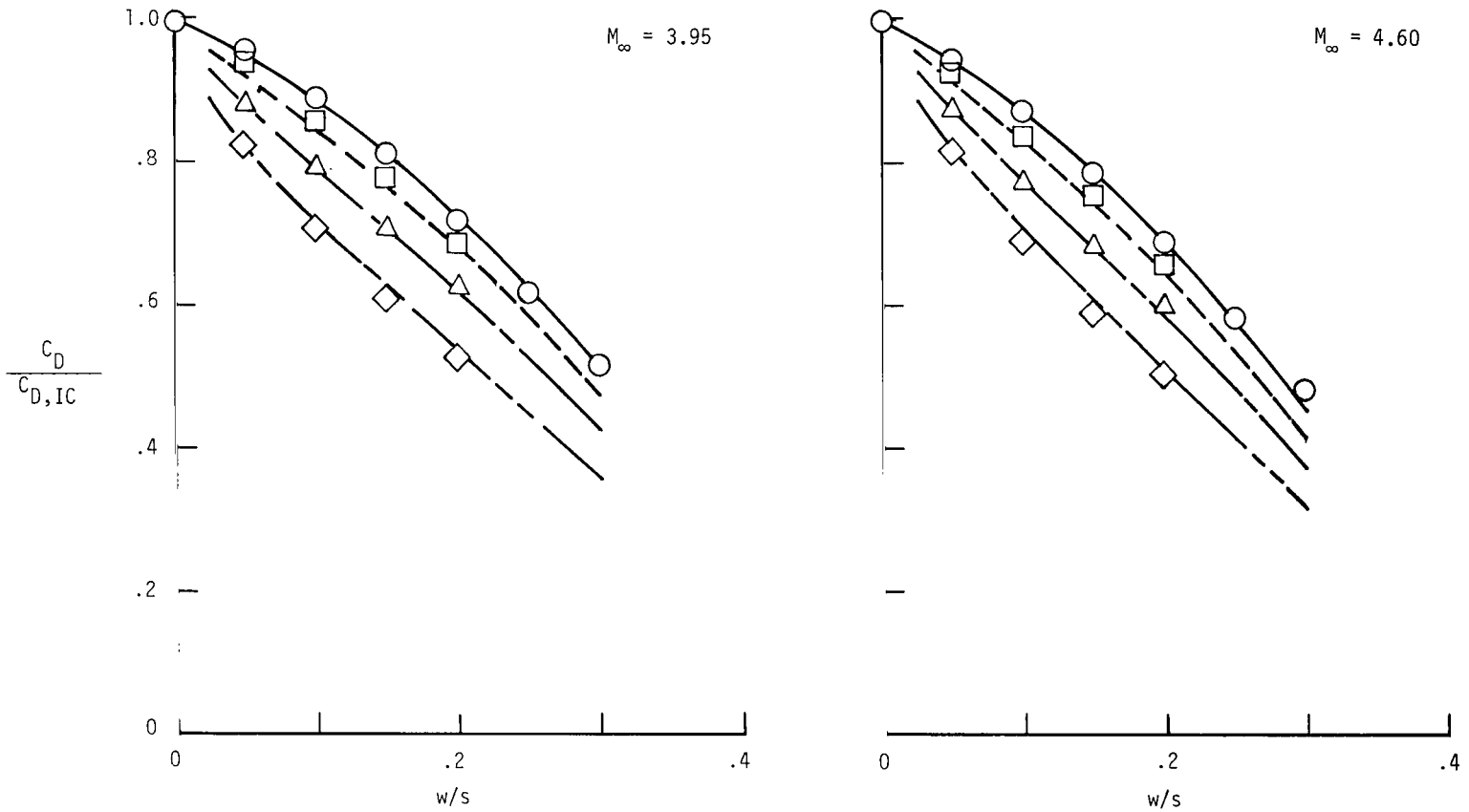

Figure 14.- Concluded.

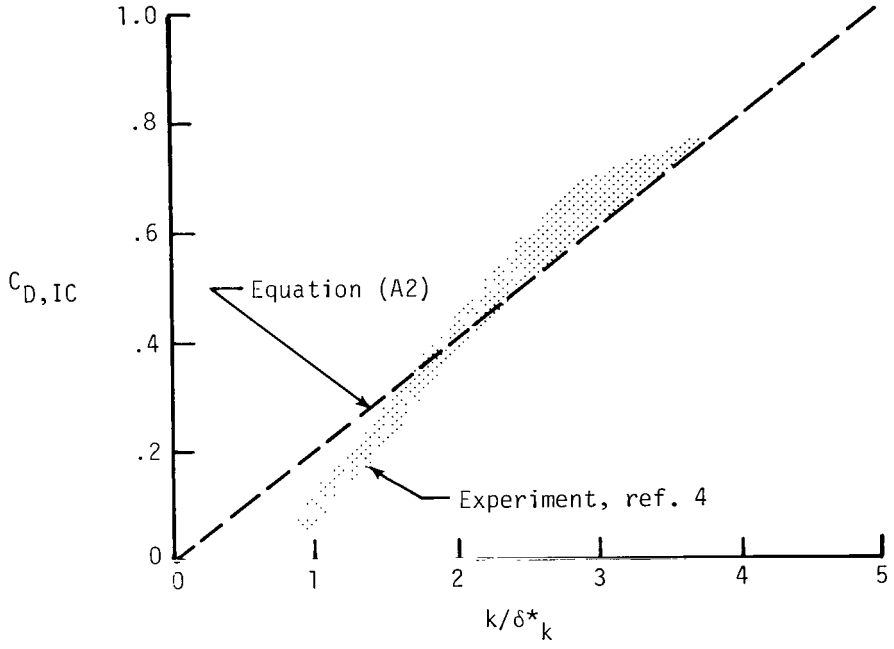

Figure 15.- Comparison of calculated and measured drag coefficients for isolated cylinder in presence of laminar boundary layer. k = w.

1. Report No.	2. Government Accession No.	3. Recipient's Catalog No.
NASA TP-1027		

4. Title and Subtitle	5. Report Date
EFFECTS OF ROUGHNESS SIZE ON THE POSITION OF BOUNDARY-LAYER TRANSITION AND ON THE AERODYNAMIC CHARACTERISTICS OF A 55° SWEPT DELTA WING AT SUPERSONIC SPEEDS	December 1977
	6. Performing Organization Code
7. Author(s)	8. Performing Organization Report No.
Robert L. Stallings, Jr., and Milton Lamb	L-11496
	10. Work Unit No.
9. Performing Organization Name and Address	505-11-15-02
NASA Langley Research Center Hampton, VA 23665	11. Contract or Grant No.
	13. Type of Report and Period Covered
12. Sponsoring Agency Name and Address	Technical Paper
National Aeronautics and Space Administration Washington, DC 20546	14. Sponsoring Agency Code

15. Supplementary Notes

16. Abstract

An experimental investigation has been conducted to determine the effects of roughness size on the position of boundary-layer transition and on the aerodynamic characteristics of a 55° swept-delta-wing model. Results are presented and discussed for wind-tunnel tests conducted at free-stream Mach numbers from 1.50 to 4.63, Reynolds numbers per meter from 3.3×10^6 to 1.6×10^7, angles of attack from -8° to 16°, and roughness sizes ranging from 0.027-cm sand grit to 0.127-cm-high cylinders. Comparisons are made with existing flat-plate data. An approximate method is derived for predicting the drag of roughness elements used in boundary-layer trips.

17. Key Words (Suggested by Author(s))	18. Distribution Statement
Boundary-layer transition Roughness drag Supersonic speeds	Unclassified – Unlimited Subject Category 02

19. Security Classif. (of this report)	20. Security Classif. (of this page)	21. No. of Pages	22. Price*
Unclassified	Unclassified	47	$4.50

* For sale by the National Technical Information Service, Springfield, Virginia 22161

NASA-Langley, 197

3 1 1U,A, 120577 S00903DS
DEPT OF THE AIR FORCE
AF WEAPONS LABORATORY
ATTN: TECHNICAL LIBRARY (SUL)
KIRTLAND AFB NM 87117